1   **Multiproxy analysis of paleoenvironmental, paleoclimatic and paleoceanographic**

2   **changes during the early Danian in the Caravaca section (Spain)**

3   Vicente Gilabert[a,*], Ignacio Arenillas[a], José A. Arz[a], Sietske J. Batenburg[b], Stuart A.

4   Robinson[c]

5   [a] Departamento de Ciencias de la Tierra, and Instituto Universitario de Investigación en Ciencias

6   Ambientales de Aragón, Universidad de Zaragoza, E-50009 Zaragoza, Spain. C/ Pedro Cerbuna

7   12, 50009 Zaragoza. vgilabert@unizar.es, ias@unizar.es, josearz@unizar.es

8   [b] Departament de Dinàmica de la Terra i de l'Oceà, Facultat de Ciències de la Terra, Universitat

9   de Barcelona, Martí i Franqués, 08028 Barcelona, Spain. sbatenburg@ub.edu

10   [c] Department of Earth Sciences, University of Oxford, South Parks Road, Oxford, OX1 3AN,

11   UK. stuart.robinson@earth.ox.ac.uk

12

13   * Corresponding author Email address: vgilabert@unizar.es

14   **ABSTRACT**

15

16   After the Chicxulub impact and mass extinction at the Cretaceous-Paleogene boundary (K-PgB),

17   ecosystems haltingly recovered under unstable conditions. An early Danian (65.9 Ma)

18   perturbation of the carbon cycle known as Dan-C2, which includes two carbon isotopic excursions

19   (CIEs), has been ascribed to inputs of greenhouse gases through large-scale volcanism of the

20   Deccan Traps. However, the relationship between Dan-C2, volcanism and environmental and

21   climatic changes during the early Danian remains ambiguous. Based on stable isotopes, calcium

22   carbonate content, magnetic susceptibility and planktic foraminifera, we present a

23   paleoenvironmental, paleoclimatic and paleoceanographic reconstruction of the early Danian

24   from the Caravaca section, Spain, one of the most complete and continuous K-PgB sections

worldwide. The paleobiological response of planktic foraminifera suggests very volatile environmental conditions during the first 230 kyr of the Danian, as reflected in the rapid succession of opportunistic/generalist blooms and episodic high occurrences of aberrant specimens. According to our age model, the Dan-C2 has been identified at the Caravaca section from 65.92 to 65.74 Ma. No evidence of strong carbonate dissolution through ocean acidification was observed in the Dan-C2 interval or the rest of the studied section, excluding the K-PgB clay bed. We find that blooms of highly eutrophic *Chiloguembelitria* and increases in aberrant planktic foraminifera coincided with a major early Danian eruptive episode of Deccan Traps (Ambelani Formation), occurring before the Dan-C2. Conversely, during both Dan-C2 CIEs, less opportunistic taxa thrived, indicating changes in the upper part of the water column. This study demonstrates that the relationship between marine biota and climate change was very complex and rapidly changing during the early Danian. In addition, we propose that the Deccan volcanism had adverse effects on marine plankton, mostly through strong eutrophication, while an increased water column stratification during the Dan-C2 event resulted in a transient boost in the recovery of ecosystems.

HIGHLIGHTS

Rapid changes among planktic foraminifera within the first 230 kyr of the Paleocene

Low carbonate dissolution in the Danian suggests low rates of volcanic CO_2 emissions

Evidence of the Dan-C2 event between 65.92 and 65.74 Ma

Dan-C2 CIEs associated with reorganization of planktic foraminiferal assemblages

1. Introduction

The Cretaceous-Paleogene boundary (K-PgB) is marked by one of the most devastating geological events that has occurred on Earth (Alvarez et al., 1980; Smit and Hertogen, 1980) caused by the impact of a ~10 km-diameter asteroid at the Yucatan Peninsula, Mexico, known as the Chicxulub asteroid (Hildebrand et al., 1991). It is widely understood that the asteroid impact caused a series of catastrophic environmental effects, including the blockage of solar radiation leading to a cold and dark "impact winter", ocean acidification, and pollution by toxic heavy metals, resulting in one of the greatest biotic crises on Earth (Kring, 2007; Premović, 2009; Schulte et al., 2010; Vellekoop et al., 2014, 2016; Gulick et al., 2019; Henehan et al., 2019; Gibbs et al., 2020). The environmental effects were lethal in the pelagic realm and caused the decimation of calcareous plankton at the K-PgB (Smit, 1982; Arenillas et al., 2000a,b; Bown, 2005). Multiple lines of evidence have pointed to the Chicxulub impact as the main cause of the K-PgB mass extinction (e.g. Smit, 1999; Arenillas et al., 2006; Schulte et al., 2010; Lowery et al., 2018; Henehan et al., 2019). Nonetheless, recent advances in radiometric dating constrain the eruptive phases of Deccan Traps volcanism (in India), as well as the Chicxulub impact, to a period of only a few hundred thousand years during magnetochron C29r (Chenet et al., 2007; Renne et al., 2015; Schoene et al. 2015, 2019; Sprain et al., 2019) thereby hindering a clear distinction between the specific roles of volcanism and impact in the K-PgB mass extinction. Consequently, these issues remain a topic of intense debate 40 years since the impact hypothesis was first proposed (Alvarez et al., 1980; Hull et al., 2020; Keller et al., 2020).

Discrepancies in the age of the K-PgB and its stratigraphic position within the Deccan Traps, as well as uncertainty regarding the eruptive rates of its main phases, result in two models of Deccan Traps eruptions, and a controversy about the role of Deccan volcanism in the K-PgB mass extinction and early Danian climate change (Burgess, 2019; Hull et al., 2020; Keller et al., 2020). Based on $^{40}Ar/^{39}Ar$ dating, and volcano-stratigraphic and biostratigraphic evidence, it has been argued that the most voluminous Deccan eruptions occurred during the early Danian,

79   corresponding to the emplacement of the Poladpur, Ambenali and Mahabaleswar Formations of

80   the Wai subgroup (Jay and Widdowson, 2008; Renne et al., 2015; Richards et al., 2015; Sprain et

81   al., 2019). However, based on U/Pb dating of the Deccan Traps Formations, it has been proposed

82   that the volcanic phase with the highest eruptive rate (Poladpur Formation) occurred in the latest

83   Maastrichtian, only tens of thousands of years prior the K-PgB (Schoene et al., 2015, 2019, 2021).

84

85   Although geochemical signatures ascribed to Deccan volcanism, such as $^{187}Os/^{188}Os$

86   excursions and Hg enrichments, have been recognized prior to the KPB (Robinson et al., 2009;

87   Font et al., 2016,2018; Keller et al., 2020), several paleo-ecological and paleoclimate studies (e.g.

88   Thibault and Gardin, 2010; Thibault et al., 2016; Hull et al., 2020; Gilabert et al., 2021) have

89   shown that the influence of the Deccan volcanism during the latest Maastrichtian did not

90   contribute to the K-PgB mass extinction (although this is disputed by some; e.g. Keller et al.,

91   2020 and references therein). A broad temporal coincidence also exists between post-K-PgB

92   Deccan volcanism and the first Danian hyperthermal event, known as Dan-C2 (Quillévéré et al.,

93   2008), which has led some to speculate that the two are mechanistically linked (e.g. Coccioni et

94   al., 2010; Punekar et al., 2014a; Krahl et al., 2020). However, others have suggested that the Dan-

95   C2 event could be astronomically controlled (Quillévéré et al., 2008; Barnet et al., 2019; Sinnesael

96   et al., 2019) and recent models of the CO_2 emission rates of Deccan volcanism suggest that

97   outgassing from Deccan volcanism alone was incapable of driving the magnitude of climate

98   change observed during the early Danian (Hull et al., 2020; Fendley et al., 2020).

99

100   During the earliest Danian, planktic foraminiferal and calcareous nannoplankton

101   assemblages were characterized by low diversity, a high single-species dominance, rapid

102   evolutionary turnovers, and blooms of smaller generalist or opportunist taxa that could thrive

103   under eutrophic and unstable conditions (Romein, 1977; Smit, 1982; Huber et al., 2002; Lamolda

104   et al., 2005; Arenillas et al., 2006; Jiang et al., 2010; Jones et al., 2019; Lowery et al., 2020).

105   Recently, it has been proposed that non-calcareous algal and microbial communities bloomed in

106   the open ocean in the short-term aftermath of the Chicxulub impact (Bralower et al., 2020).

107   According to Bralower et al. (2020), these microbial blooms probably contributed to rapid

108   ecosystem recovery by removing nutrients and providing a food source for higher trophic orders,

109   enhancing pelagic ocean habitability as evidenced by the rapid recovery of planktic foraminifera

110   and calcareous nannoplankton after the impact.

111

112   The main planktic foraminiferal indicators of enhanced environmental stress across the K-

113   PgB are the guembelitriid blooms (Kroon and Nederbragt 1990; Keller and Pardo, 2004; Pardo

114   and Keller, 2008; Ashckenazi-Polivoda et al., 2014; Punekar et al., 2014a,b) and the increases in

115   aberrant planktic foraminifera tests (Gerstel et al., 1986; Coccioni and Luciani, 2006; Arenillas

116   et al., 2018). Worldwide, blooms of *Guembelitria* and its descendant *Chiloguembelitria* have been

117   reported well above the K-PgB (Arenillas et al., 2018), and thus appear genetically disconnected

118   from the Chicxulub impact. However, the blooms did occur within the temporal range of Deccan

119   volcanism in the Danian which points to a potential cause and effect relationship (Keller et al.,

120   2012; Punekar et al., 2014a,b; Arenillas et al., 2018). Similarly, an increase in aberrant

121   foraminifera tests after the K-PgB has been shown to continue locally at the El Kef and Aïn

122   Settara sections (Tunisia) for several hundreds of thousands of years after the K-PgB (Arenillas

123   et al., 2018), suggesting the persistence of stressed conditions.

124

125   Except for the immediate aftermath of the Chicxulub impact, the climatic and environmental

126   changes that occurred during the first thousand years of the Danian leading up to the Dan-C2

127   event have not been exhaustively examined (e.g., Quillévéré et al., 2008; Barnet et al., 2019). To

128   improve our understanding of the complex paleobiological changes that took place during the

129   early Danian, and their potential relationship with the Deccan volcanism and the Dan-C2 event,

130   we carried out a detailed analysis of the first ~750 kyr of the Danian at the Caravaca section (SE

131   Spain, western Tethys). We took a multi-proxy approach: quantitative, diversity, taphonomic

132   (fragmentation index) and teratological (percentage of aberrant specimens) analyses of planktic

133   foraminifera, as well as bulk geochemical (stable C- and O-isotopes, $CaCO_3$ content) and

134   magnetic susceptibility measurements. Caravaca is a well-known section for its excellent

135 exposure, completeness and continuity (Smit, 1982, 2004; Molina et al., 2009), and provides an

136 exceptional opportunity to evaluate paleoclimatic, paleoceanographic and paleobiological

137 changes during the early Danian.

138

139 **2. Material and methods**

140

141   We revisited the Caravaca section, which is located in the Barranco del Gredero (38º04'36"

142 N, 1º52'42" W), southwest of Caravaca de la Cruz, SE Spain (Fig. 1). The Danian part of this

143 section consists mostly of hemipelagic marly limestones (Fig. 2), although it starts with the well-

144 known K-PgB clay bed (Smit, 1982, 2004), consisting of a 1-2 mm-thick red air-fall layer and a

145 6 cm-thick dark clay bed, that is almost black in the lowermost 1.5 cm (Fig. 1E). This section was

146 chosen as an auxiliary section of the Global Boundary Stratotype Section and Point (GSSP) for

147 the base of the Danian Stage (Molina et al., 2009), as it represents one of the most continuous and

148 complete K-PgB sections worldwide (Smit and Hertogen, 1980; Smit and Romein, 1985).

149 Previous studies have focused on the K-PgB clay bed and the first one or two meters of the

150 lowermost Danian, with a significantly lower resolution above this interval (Smit, 1982, 2004;

151 Canudo et al., 1991; Coccioni and Galeotti, 1994; Kaiho and Lamolda, 1999; Arz et al., 2000;

152 Lamolda et al., 2005; Vellekoop et al., 2018; Sepúlveda et al., 2019). In contrast, we sampled the

153 first 820 cm of the Danian at high resolution, taking samples every 1-5 cm over the first 200 cm,

154 and every 25-30 cm across the rest of the section.

155
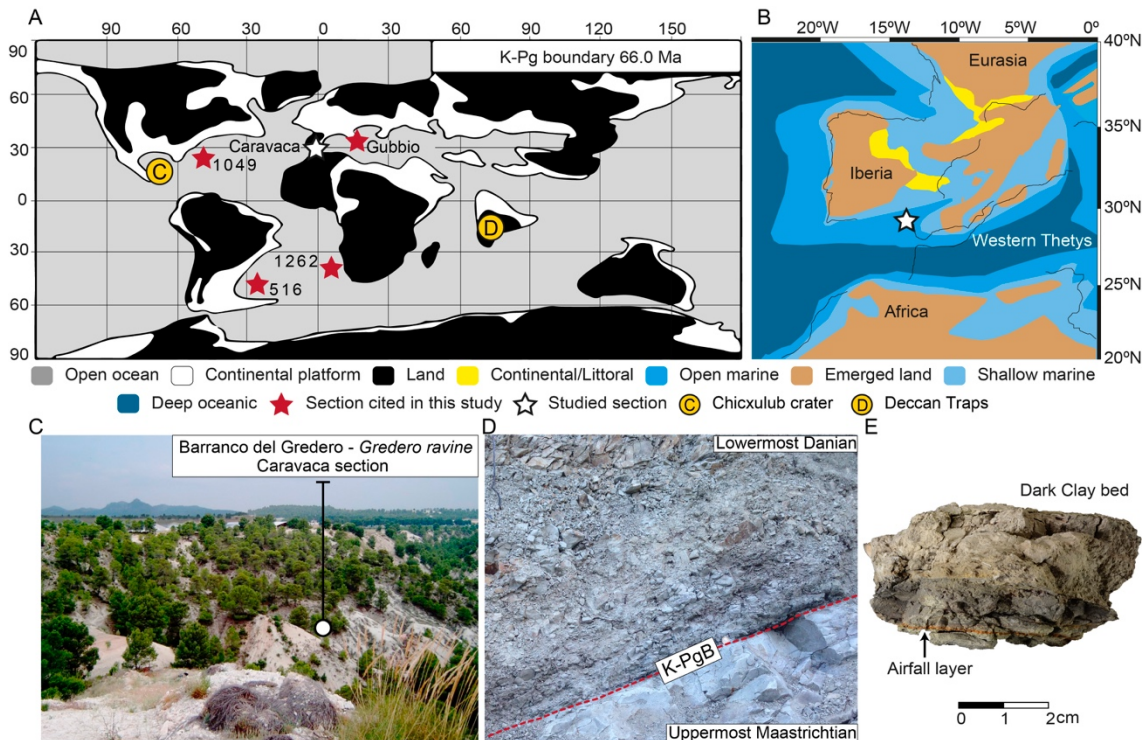
Fig. 1. A) Paleogeographical location map of Caravaca and other localities worldwide: DSDP Site 516, ODP Sites 1262 and 1049, and Gubbio (Contessa Highway section). B) Detailed paleogeographical map of the Western Tethys, with the star indicating the position of Caravaca (modified from Andeweg, 2002). C) Caravaca section overview. D) Detail of the Cretaceous-Paleogene transition. E) Rock fragment of the first 3 centimeters of the K-PgB clay bed at Caravaca, which includes the 1-2 mm thick ejecta-rich air-fall layer and the basal part of dark clay bed.

2.1. Micropaleontological methods

For micropaleontological analyses, a total of 46 samples were disaggregated in H_2O_2 for 3-4 hours. These samples were washed and sieved under running water; the size fraction >63 microns was collected, and the residue was oven-dried at 50 °C for 24 h. Representative splits of ca. 300 individuals per sample were studied for quantitative analyses, classifying the specimens at species level. Representative specimens from Caravaca were photographed with a JEOL JSM 6400 SEM (scanning electron microscope) at the Microscopy Service of the Universidad de Zaragoza (Spain).

174

175   For the Danian, we have used the planktic foraminiferal zonation of Arenillas et al. (2004),

176 which was updated by Metsana-Oussaid et al. (2019). In Fig. 2, this biozonation has been

177 compared with the more standardized zonation of Berggren and Pearson (2005), which was

178 revised by Wade et al. (2011). Although the taxonomy used by the authors differs, the close

179 correspondence of biozones and subbiozones is illustrated in Fig. 2. The stratigraphic distribution

180 of Danian planktic foraminiferal species across the Caravaca section is also illustrated in Fig. 2.

181 SEM photographs of index-species and other relevant Danian species are displayed in Fig. 3.

182

183

184

8
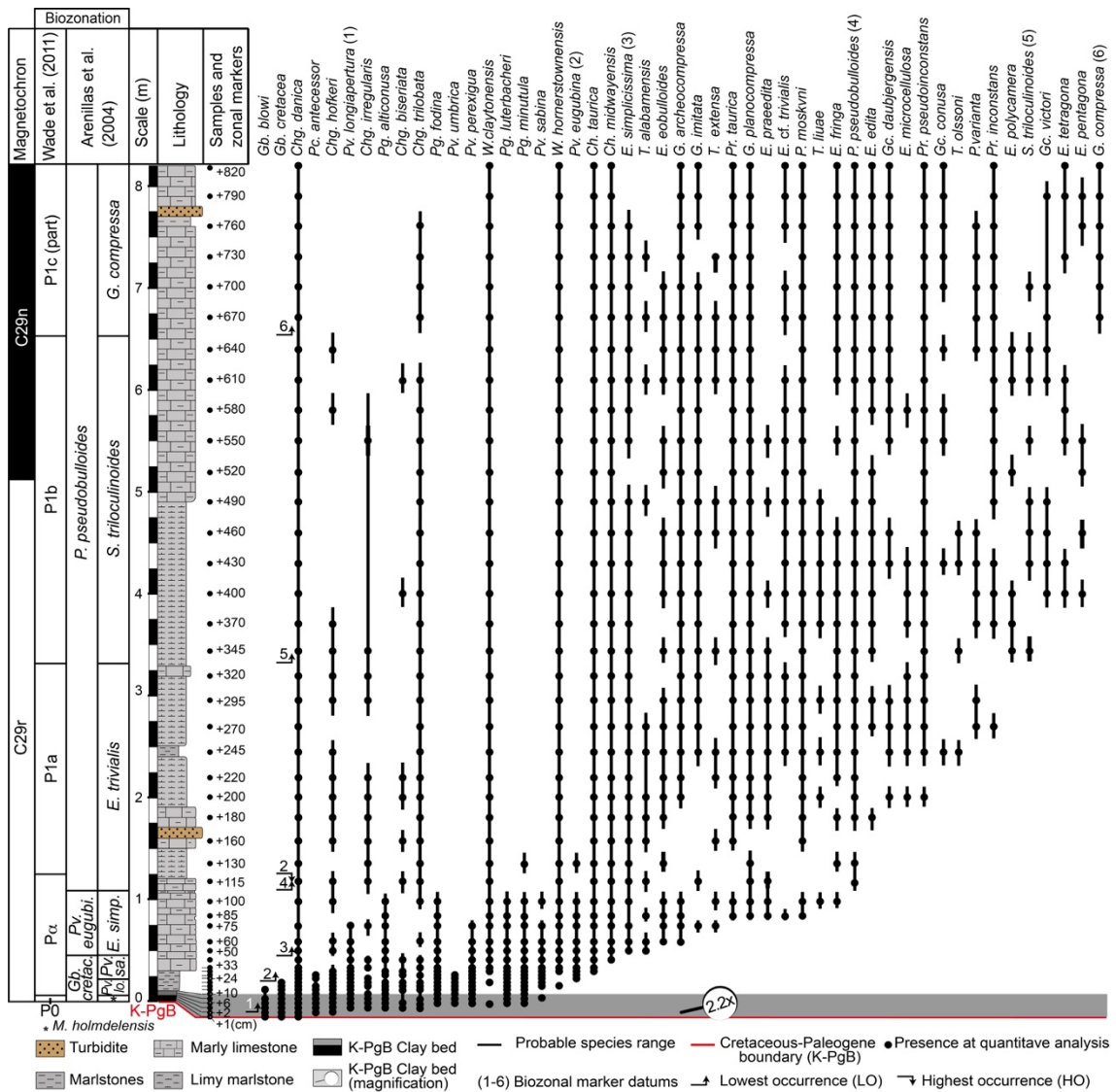
185   Fig. 2. Stratigraphic column and distribution of the Danian species at Caravaca. *Gb. = Guembelitria; Chg.=*

186   *Chiloguembelitria; Pc. = Pseudocaucasina; Pg. Palaeoglobigerina; Pv.= Parvularugoglobigerina; W.=*

187   *Woodringina; Ch. = Chiloguembelina; E.= Eoglobigerina; T.= Trochoguembelitria; G.= Globanomalina;*

188   *P.= Parasubbotina; Pr.= Praemurica; Gc.= Globoconusa; S.= Subbotina.*

189
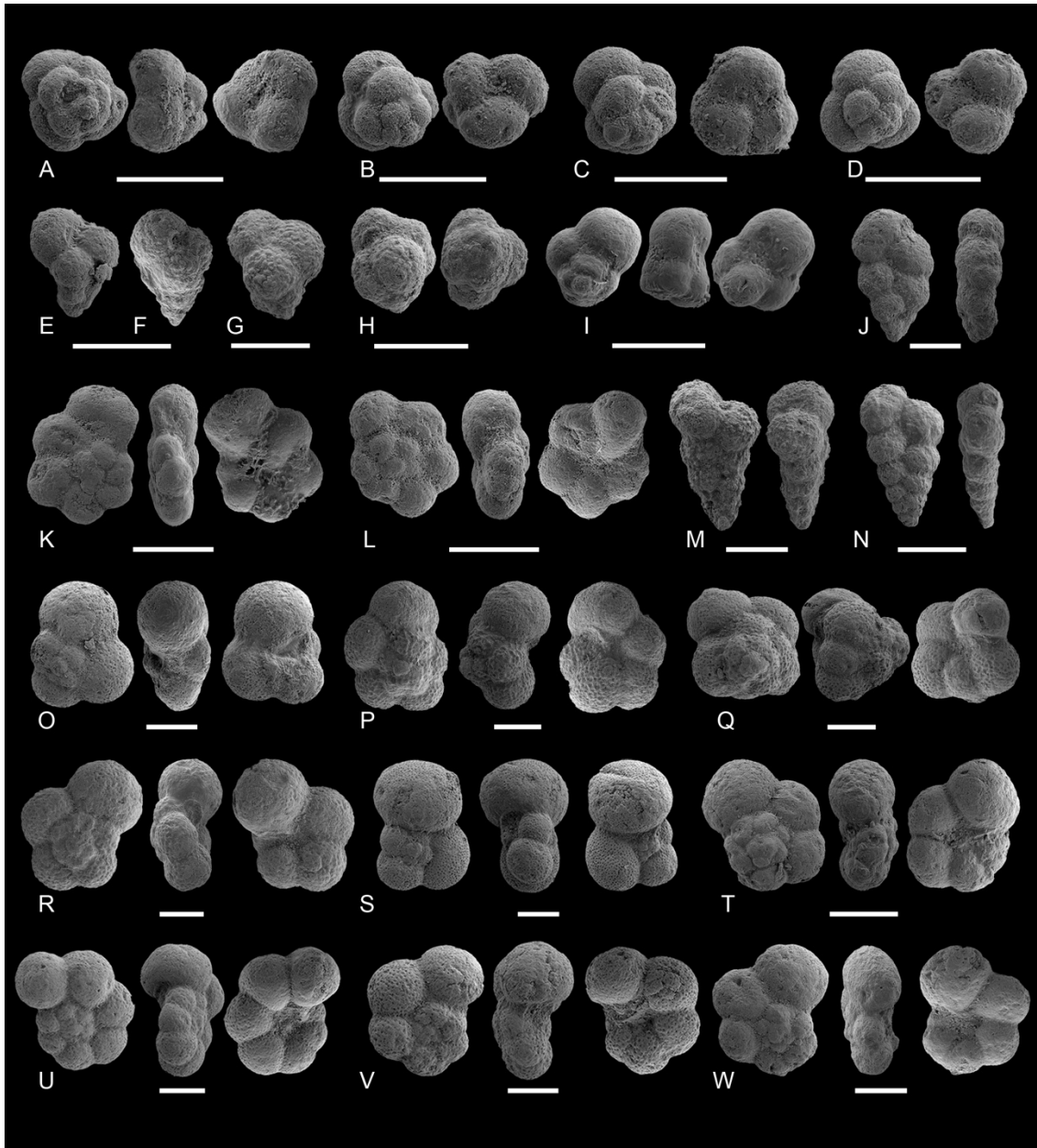
190

191

192   Fig. 3. SEM photographs of *Pseudocaucasina antecessor* (A-D); *Guembelitria cretacea* (E);

193   *Chiloguembelitria hofkeri* (F); *Chiloguembelitria danica* (G); *Trochoguembelitria alabamensis* (H);

194   *Palaeoglobigerina alticonusa* (I); *Chiloguembelina midwayensis* (J); *Parvularugoglobigerina*

195 *longiapertura* (K); *Parvularugoglobigerina eugubina* (L); *Woodringina hornerstownensis* (M);

196 *Chiloguembelina taurica* (N); *Eoglobigerina simplicissima* (O); *Eoglobigerina edita* (P); *Eoglobigerina*

197 *pentagona* (Q); *Parasubbotina pseudobulloides* (R); *Subbotina triloculinoides* (S); *Globanomalina*

198 *archeocompressa* (T); *Praemurica taurica* (U); *Praemurica inconstans* (V); *Globanomalina compressa*

199 (W). White bar scales = 100 microns.

200

201   To identify the planktic foraminiferal acme-stages (PFAS) proposed by Arenillas et al.

202 (2006) for the lower Danian, we used quantitative data (Tables S1, S2) and the PAST software

203 (v4.0.3, Hammer et al., 2001) for R-mode cluster analyses using the well-known Bray-Curtis

204 index. We chose The Bray-Curtis similarity index since it is a more appropriate index for

205 abundance data (i.e. species assemblages) than other distance measures, such as the common

206 Euclidian distance (Beals, 1984; Ricotta and Podani, 2017). The Euclidean distance can lead to

207 misleading results when species abundance data contains zeros (i.e. absences of certain taxa) as

208 this method places more weight on the abundance differences between samples than on the

209 similarities in the assemblage of species (Legendre and Gallagher, 2001). In contrast, in the Bray-

210 Curtis index common and scarce species have relatively similar weights, which means that the

211 assemblage (as opposed to the absolute abundances) becomes the more significant control on

212 distance (Ricotta and Podani, 2017). The criteria for distinguishing the boundaries between PFAS

213 are clear: PFAS-1 is characterized by a dominance of triserial guembelitriids (*Guembelitria*),

214 PFAS-2 by the tiny trochospiral parvularugoglobigerinids (*Parvularugoglobigerina* and

215 *Palaeoglobigerina*), and PFAS-3 by biserial *Woodringina* and *Chiloguembelina*. All three acme-

216 stages, first recognized in the Spanish sections of Zumaia (Arenillas et al., 1998) and Agost

217 (Molina et al., 1998), have been identified in lower Danian sections worldwide (Arenillas et al.,

218 2006, 2016; Gallala et al., 2009; Lowery et al., 2018; Renne et al., 2018).

219

220   To reconstruct paleo-environmental change, we have used several planktic foraminiferal

221 proxies: paleoecological preferences of species, the abundance of aberrant specimens,

222 fragmentation index, diversity indices and the planktic/benthic ratio. Early Danian planktic

10

223   foraminiferal paleoecology has previously been interpreted based on the isotopic signatures of

224   each species (e.g. Olsson et al., 1999; Aze et al., 2011; Birch et al., 2012). In order to discriminate

225   between normal and abnormal specimens, we followed the compendium of aberrant

226   morphologies of Arenillas et al. (2018) for early Danian planktic foraminifera. The fragmentation

227   index (ratio of broken vs. complete foraminifers) was calculated following the method of Berger

228   et al. (1982), and used to identify changes in carbonate preservation state. Benthic foraminifers

229   were picked to evaluate potential dissolution processes by calculating the planktic/benthic (P/B)

230   ratio (% planktic foraminifera of the total number of foraminifera), but they were not

231   taxonomically classified.

232

233   *2.2 Geochemical and geophysical methods.*

234

235   The inorganic and organic carbonate content was measured using duplicate subsamples from

236   70 samples that were weighed into ceramic boats, one of which was roasted in air at 420˚C for 12

237   hours to remove organic carbon. The total carbon content (TC) of the unroasted subsample, and

238   the Total Inorganic Carbon (TIC) of the roasted subsample, were determined using a Strohlein

239   Coulomat 702, in the Department of Earth Sciences of the University of Oxford. The difference

240   between the amount of carbon determined in unroasted and pre-roasted samples provided an

241   estimate of Total Organic Carbon (TOC). Assuming the inorganic carbon content is all associated

242   with $CaCO_3$ allows the estimation of $CaCO_3$ content using the equation from Stax and Stein

243   (1993): $CaCO_3\% = TIC * 8.33$. Reproducibility of %C using this method is typically better than

244   0.1%.

245

246   Measurements of stable carbon and oxygen isotope ratios ($\delta^{13}C$, $\delta^{18}O$) were performed on

247   homogenized bulk powdered sediment from the same 70 samples. Samples were analyzed in the

248   Department of Earth Sciences of the University of Oxford using a GasBench device attached to a

249   ThermoFisher Delta V Advantage gas source isotope ratio mass spectrometer. Oxygen and

250   carbon-isotopes are reported using the standard delta notation ($\delta^{18}O$, $\delta^{13}C$) in parts per mil (‰)

on the Vienna PeeDee Belemnite (VPDB) scale. Calibration of samples to the VPDB scale was achieved using multiple analyses of an in-house standard, NOCZ, which has average values on the VPDB scale of -1.90‰ for $\delta^{18}O$ and 2.18‰ for $\delta^{13}C$. For $\delta^{18}O$, NOCZ has been calibrated to the VPDB scale by comparison with analyses of NBS-19 and NBS-18, which were assigned $\delta^{18}O$ values of -2.20‰ and -23.01‰ respectively. For $\delta^{13}C$, NOCZ has been calibrated to the VPDB scale by comparison with analyses of NBS-19, which was assigned a value of 1.95‰. Repeated analyses of in-house standards suggest a reproducibility ($\pm 1\sigma$) of <0.1 for both $\delta^{13}C$ and $\delta^{18}O$.

The magnetic susceptibility (MS) of 70 samples was measured at the University of Zaragoza, Spain, with a Spinning Specimen Magnetic Susceptibility Anisotropy Meter KLY-35 Kappabridge. Samples were crushed in an agate mortar and measured in cylindrical plastic boxes of 10 cm³ in volume. MS values are reported relative to mass (m^3/kg).

3. Results

3.1. Biostratigraphy and age model

At the Caravaca section, a total of 49 species and 14 genera of Danian planktic foraminifera (including species of the genus *Guembelitria*) have been identified. Relative abundances of each species are shown in the Supplementary Table 1. Seven subbiozones have been identified: *Mh. holmdelensis* and *Pv. longiapertura* Subzones (of the *G. cretacea* Zone), *Pv. sabina* and *E. simplicissima* Subzones (of the *Pv. eugubina* Zone), and *E.* cf. *trivialis*, *S. triloculinoides* and *G. compressa* (part) Subzones (of the *P. pseudobulloides* Zone). The stratigraphic interval studied corresponds to Pα, P1a, P1b and (part of) P1c of Berggren and Pearson (2005) and Wade et al. (2011). At Caravaca, the bases of these subbiozones are at 0, 3, 22, 42, 107, 332 and 655 cm, respectively, above the K-PgB (Fig. 2).

278   To establish the age model at the Caravaca section, we linearly interpolated between the K-

279   PgB, the top of the K-PgB dark clay bed, the C29r/C29n magnetic reversal and the C29n/C28r

280   magnetic reversal. Based on the ^{40}Ar/^{39}Ar calibrations of Sprain et al. (2018), we have assigned

281   an age of 66.052 Ma to the K-PgB, 65.724 Ma to the C29r/C29n reversal and 65.075 Ma to the

282   C29n/C28r reversal. Based on cosmic ^{3}He sedimentation rates, Mukhopadhyay et al. (2001)

283   estimated a duration for deposition of the K-PgB dark clay bed of ~10 kyr. At Caravaca, the top

284   of the K-PgB dark clay bed is ~6 cm above the K-PgB, and, according to Smit (1982) and Groot

285   et al. (1989), the C29r/C29n and C29n/C28r reversals are at 5.1 m and 9.8 m above the K-PgB

286   respectively. Consequently, the average sedimentation rates at Caravaca are ~0.6 cm/kyr for the

287   K-PgB dark clay bed, 1.58 cm/kyr for the Danian part of C29r and 0.72 cm/kyr for C29n. In total,

288   the studied section spans approximately the first 760 kyr of the Danian. According to this age

289   model, the bases of *Mh. holmdelensis*, *Pv. longiapertura*, *Pv. sabina, E. simplicissima, E.* cf.

290   *trivialis*, *S. triloculinoides* and *G. compressa* Subzones occurred at 0, 5, 20, 33, 75, 219, and 528

291   kyr after the K-PgB, respectively. It is remarkable that *Pseudocaucasina antecessor* (Arenillas

292   and Arz, 2017) has been identified at Caravaca for the first time. Its Lowest Occurrence Data

293   (LOD) is at 1.5 cm above the K-PgB, i.e. 2.5 kyr after the K-PgB. The LODs of its most direct

294   evolutionary descendants, *Parvularugoglobigerina longiapertura* and *Palaeoglobigerina*

295   *alticonusa*, are at 3 cm above the K-PgB, i.e. 5 kyr after the K-PgB.

296

297   *3.2. Acme-stratigraphy*

298

299   Planktic foraminiferal assemblages identified in the lower Danian of the Caravaca section

300   are characterized by low diversities and high consecutive dominances of single taxon groups,

301   corresponding to the succession of the three acme-stages PFAS of Arenillas et al. (2006). This is

302   confirmed by the cluster analysis performed here (Fig. 4).

303

304   PFAS-1 spans the first 5 cm of the lower Danian of the Caravaca section (from the K-PgB

305   to the lowermost part of *Pv. longiapertura* Subzone), i.e. the first 8 kyr after the K-PgB boundary

306   according to our age model. PFAS-1 is dominated by triserial taxa, mainly *Guembelitria* and, to

307   a lesser extent, its descendant *Chiloguembelitria. Guembelitria* is the only Cretaceous genus that

308   increased its abundance after the K-PgB. In addition, we have identified a bloom of

309   *Pseudocaucasina antecessor*, which starts within the PFAS-1 and ends at the lowermost part of

310   PFAS-2. (Fig. 5, Table S1).

311

312   PFAS-2 is placed at 5 to 55 cm above the K-PgB at Caravaca (from the lowermost part of

313   *Pv. longiapertura* Subzone to the middle part of the *E. simplicissima* Subzone), i.e. between 8

314   and 41 kyr after the K-PgB. This acme-stage is dominated by parvularugoglobigerinids, i.e.

315   *Parvularugoglobigerina* and *Palaeoglobigerina* (the first evolutionary radiation of Danian

316   species), comprising between 50 and 80% of the assemblages. The LODs of *Woodringina* and

317   *Chiloguembelina*, the first Danian biserial taxa, occurred within PFAS-2, but their combined

318   relative abundance never exceeds 3% except for the upper part of PFAS-2. Around 38 cm above

319   the K-PgB (upper part of the *Pv. sabina* Subzone), biserial taxa show a sharp increase, but they

320   do not exceed the parvularugoglobigerinids in abundance.

321

322   PFAS-3 has been recognized from 55 cm above the K-PgB to the top of the studied section

323   (from the lower part of the *E. simplicissima* Subzone to the lower part of the *G. compressa*

324   Subzone), i.e. between 41 kyr and at least 756 kyr after the K-PgB. The planktic foraminiferal

325   assemblages in PFAS-3 comprise mostly biserial taxa, i.e. the genera *Woodringina* and

326   *Chiloguembelina*, and especially the species *Woodringina hornerstownensis* (30.7% on average).

327   Although PFAS-3 assemblages are dominated by biserial taxa throughout, several substages can

328   be identified on the basis of changes in relative abundances of some other taxa. One of the most

329   striking features within PFAS-3 at Caravaca is the occurrence of three successive blooms of the

330   opportunist triserial *Chiloguembelitria* reaching maxima abundances of 48.5, 28.6, and 12.3%

331   respectively. These *Chiloguembelitria* blooms are successively less intense and alternate in time

332   with remarkable increases in the combined abundance of genera resulting from the second Danian

333   evolutionary radiation, including *Eoglobigerina*, *Parasubbotina*, *Globanomalina*, *Praemurica*,

and *Subbotina,* or "other genera" for short. The latter group reaches maxima abundance values of

335 43.1, 49.5 and 48.4% between each *Chiloguembelitria* bloom (Fig. 5). Cluster analyses strongly

336 support the further division of PFAS-3 into 7 shorter substages following the alternation of major

337 groups (Fig. 4), with each substage named as PFAS-3 plus a suffix: α, T1, O1, T2, O2, T3, O3.

338 Stratigraphic and temporal boundaries of each stage and substage, with average relative

339 abundances of major groups are listed in Table 1.

340
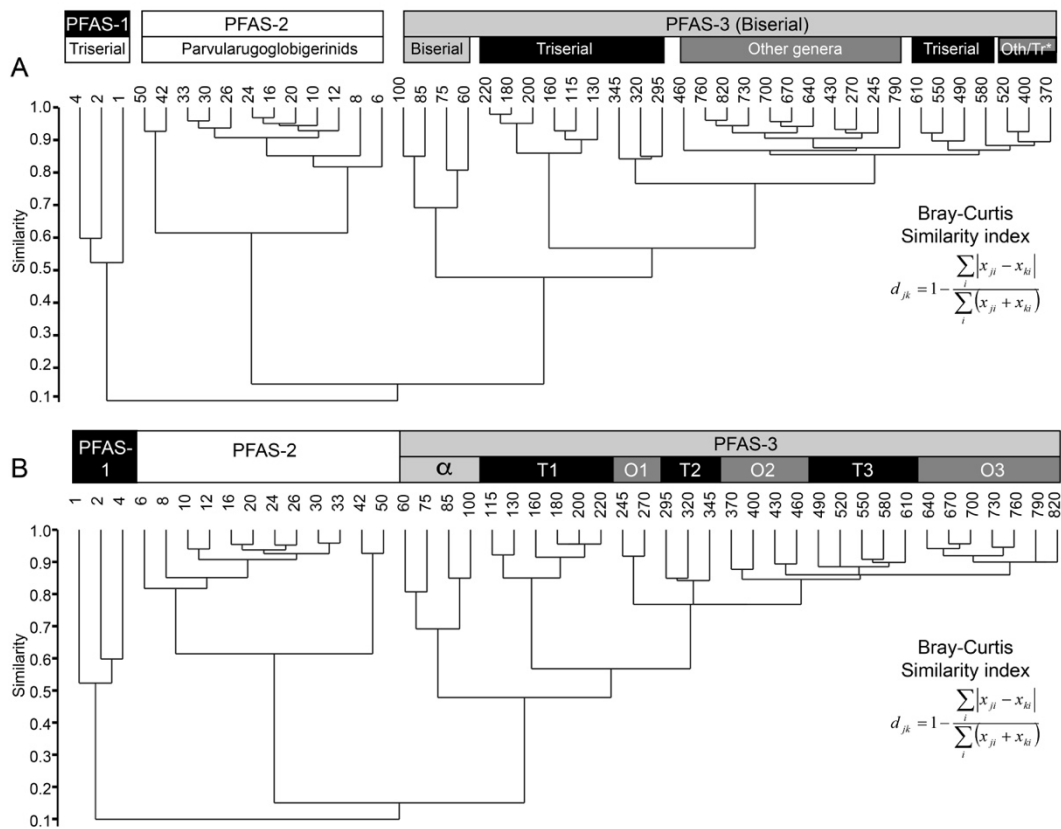
341

342 Fig. 4. A) Agglomerative clustering based on the unweighted paired group method with the arithmetic mean

343 (UPGMA) and the Bray-Curtis similarity index. Oth/Tr*. = Clusters with ambivalent affinity. B)

344 Stratigraphically constrained dendrogram.

345

346

Table 1. Stratigraphic height and age of PFAS and relative abundance of major groups

PFAS	Height from K-PgB (cm)		Age from K-PgB (kyr)		Major groups relative abundance (%)			
	Base	Top	Base	Top	Triserial	Parvul.	Biserial	Others

PFAS-3O3	625	820*	487	756*	2.3%	0.0%	56.9%	40.8%
PFAS-3T3	475	625	311	487	8.8%	0.0%	59.5%	31.7%
PFAS-3O2	357	475	235	311	6.6%	0.0%	53.6%	39.8%
PFAS-3T2	282	357	187	235	21.4%	0.0%	58.8%	19.8%
PFAS-3O1	232	282	155	187	2.4%	0.0%	55.6%	41.9%
PFAS-3T1	107	232	75	155	45.2%	0.0%	49.0%	5.8%
PFAS-3α	55	107	41	75	0.8%	24.7%	67.0%	7.5%
PFAS-2	5	55	8.3	41	9.7%	83.4%	6.8%	0.1%
PFAS-1	K-PgB	5	0	8.3	76.1%	23.1%	0.9%	0.0%

Table 1. Stratigraphic position and calibrated age of planktic foraminiferal acme-stages (PFAS) at Caravaca, and relative abundances of the major planktic foraminiferal groups. * = Top of the studied section. Parvul.=Parvularugoglobigerinids

PFAS-3α is characterized almost exclusively by biserial *Woodringina* and *Chiloguembelina,* but mostly by *Woodringina* (Fig. 5). The LODs of *Eoglobigerina*, *Parasubbotina*, *Globanomalina*, *Praemurica* and *Trochoguembelitria* are at 55-85 cm above the K-PgB, forming the second evolutionary radiation of Danian species (Fig. 2 and Fig. 5). The Highest Occurrence Data (HOD) of *Palaeoglobigerina* and *Parvularugoglobigerina* are recognized towards the top of PFAS-3α, as these species were completely replaced by the incoming species of the second Danian evolutionary radiation.

PFAS-3T (1-3) are characterized by subsequent blooms of triserial *Chiloguembelitria*. PFAS-3T1 witnessed the LOD of the genus *Globoconusa*, which occupies the same ecological niche as *Guembelitria* and *Chiloguembelitria* (see Olsson et al., 1999), although during each *Chiloguembelitria* bloom the relative abundance of *Globoconusa* remains extremely low with values <1% (0.1, 0.2, and 0.9%).

PFAS-3O (1-3) refers to the substages characterized by the higher relative abundance of the "other genera" combination. The genera *Globanomalina* (15.2%) and *Praemurica* (9.9%) are the

368 most abundant genera during each PFAS-3O. It is noteworthy that the alternations between PFAS-

369 3T and PFAS-3O occurred rapidly, especially between the first three alternations: T1-O1, O1-T2,

370 and T2-O2 (Fig. 5 and Tables 1, 2).

371
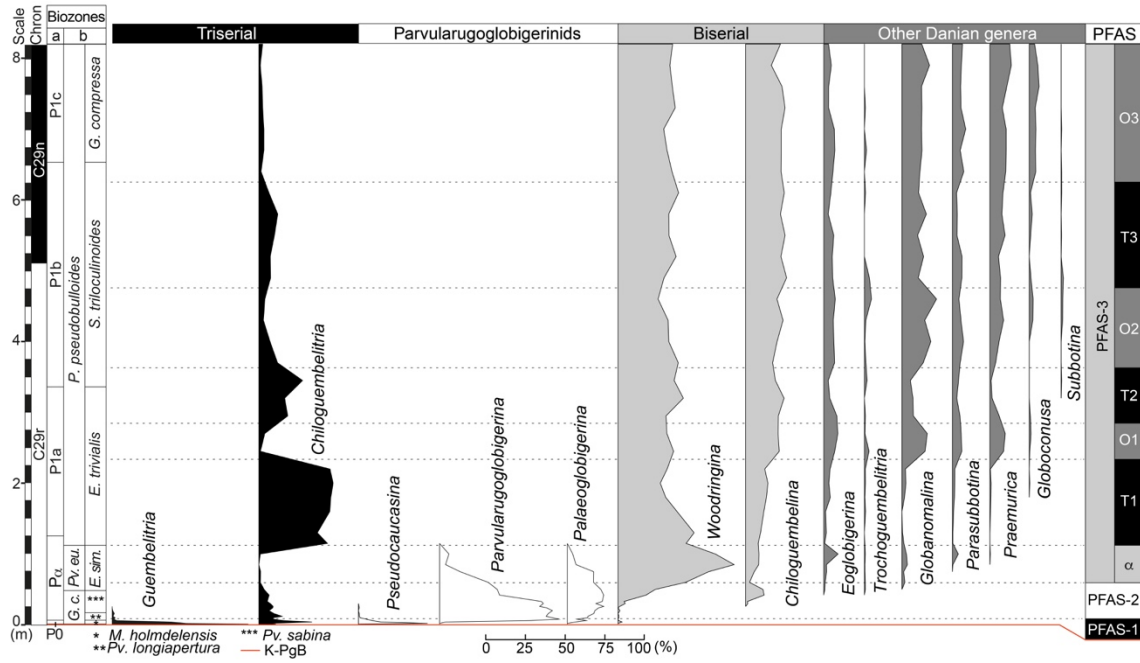
373 Fig. 5. Relative abundance of the Danian planktic foraminiferal genera and major groups at Caravaca.

374 Biozones: a = (Wade et al., 2011); b = (Arenillas et al., 2004).

375

376 *3.3. Diversity indices.*

377

378 Standard diversity indices are summarized in Table 2 and shown in full in Table S2. We have

379 calculated the average diversity values for PFAS-1-2 and for each substage of PFAS-3. The

380 diversity indices provide evidence for rapid and abrupt environmental changes from PFAS-1 to

381 the end of PFAS-3T1 (suggesting less resilient planktic foraminiferal assemblages), and more

382 stable environmental conditions from PFAS-3O1 onwards (suggesting more resilient

383 assemblages). However, it is noteworthy that the rapid evolutionary radiations which occurred

384 during the PFAS-2 and PFAS-3α intervals (Figs. 2 and Fig. 5) highly influenced the values of the

385 diversity indices. Conversely, from the base of PFAS-3O1 to the top of the section, diversity

386 indices show more gradual changes, showing slightly higher average diversity values in PFAS-

387 3O substages than in the PFAS-3T substages (see Table 2).

388

389

Table 2. Diversity indices and relative abundance of aberrant forms of major groups in each PFAS

PFAS	Main diversity indices				Relative abundance of aberrant forms (%)				
	S	H´	1/λ	E	Triserial	Parvul.	Biserial	Others	Total
PFAS-3O3	23	2.42	6.86	0.48	0.0%	0.0%	1.3%	1.3%	2.6%
PFAS-3T3	23	2.37	6.91	0.47	0.4%	0.0%	1.9%	1.4%	3.7%
PFAS-3O2	26	2.55	8.09	0.49	0.2%	0.0%	2.2%	1.7%	4.1%
PFAS-3T2	24	2.31	6.60	0.42	2.8%	0.0%	5.1%	2.2%	10.0%
PFAS-3O1	25	2.54	8.46	0.52	0.2%	0.0%	2.9%	2.4%	5.5%
PFAS-3T1	18	1.95	4.86	0.41	6.9%	0.0%	5.1%	0.5%	12.5%
PFAS-3α	20	1.88	4.24	0.33	0.0%	1.3%	4.6%	0.7%	6.6%
PFAS-2	15	1.71	3.95	0.40	1.0%	9.0%	0.7%	0.7%	11.5%
PFAS-1	6	1.26	3.13	0.64	17.3%	3.7%	0.0%	0.0%	21.0%

390

391 Table 2. Average values of main diversity indices for each planktic foraminiferal acme-stage (PFAS), and

392 relative abundance of the aberrant forms in total, and in each major group. S = Species richness; H '=

393 Shanon-Weaver index; 1/λ.= Inverse Simpson index; E = Evenness; Parvul. = Parvularugoglobigerinids

394

395 *3.4. Aberrant index*

396

397 We have found abnormal specimens of *Guembelitria* and almost every incoming Danian

398 species (Supplementary Table S3), whereas reworked Cretaceous specimens within Danian

399 sediments display almost no aberrations. According to the terminology of Arenillas et al. (2018),

400 the most common aberrant morphologies identified at Caravaca are: 1) chamber abnormalities:

401 aberrant chamber shapes, reduced chamber sizes and overdeveloped chamber sizes; 2) an

402 abnormal ultimate chamber: aberrant shape, anomalous position and bulla-like chamber; 3)

18

403   multiple ultimate chambers: double or twinned ultimate chambers, and a proliferation of

404   chambers; 4) distortion in test coiling; 5) abnormal tests. Some examples of these aberrations are

405   illustrated in Fig. 6. The aberrant forms of planktic foraminifera are mainly abundant within the

406   first 357 cm (~230 kyr) of the Danian (i.e. from the K-PgB to the top of PFAS-3T2), close to the

407   base of the *S. triloculinoides* Subzone (Fig. 7).

408
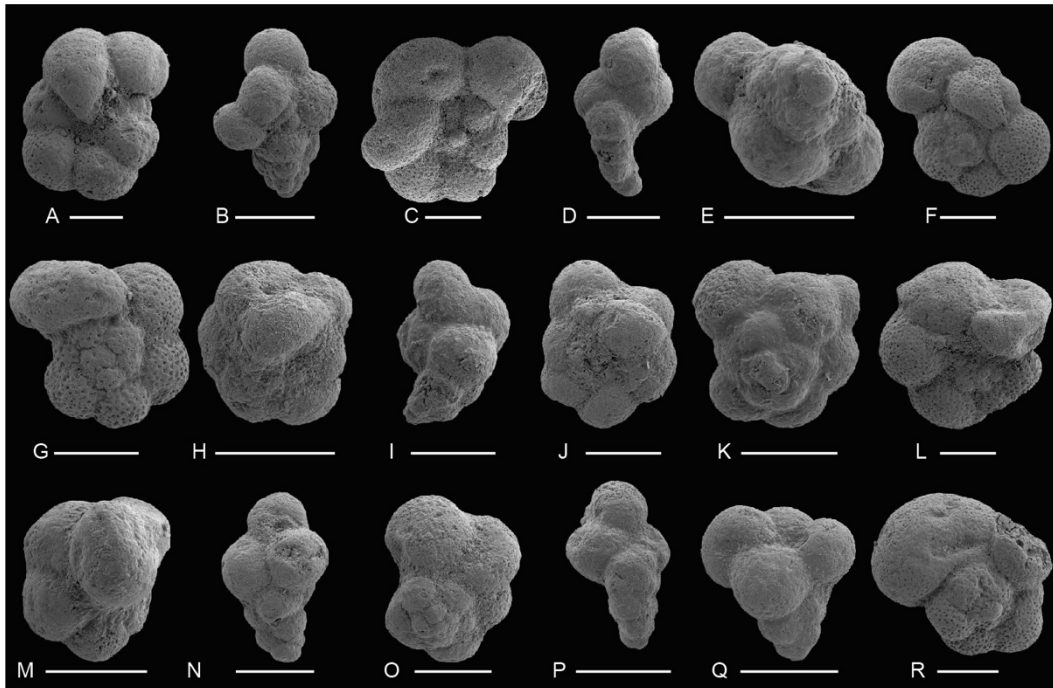
409

410

411   Fig. 6. Examples of different aberrant morphologies within the studied specimens; (A) overdeveloped

412   chamber size; (B) protuberant chamber; (C) aberrant shape; (D) overdeveloped chamber size + anomalous

413   position; (E) proliferation of chambers; (F) aberrant chamber shape; (G) abnormal ultimate chamber; (H)

414   bulla-like chamber; (I) distortion in test coiling and reduced ultimate chamber size; (J) additional chamber;

415   (K) abnormal test; (L) abnormal ultimate chamber; (M) bulla-like chamber; (N) chamber in anomalous

416   position; (O) abnormal test; (P) ultimate chambers in anomalous position and distortion in test coiling; (Q)

417   proliferation of chambers; (R) overdeveloped ultimate chamber with aberrant shape.

418

419   PFAS-1 and PFAS-2 are characterized by high relative abundances of aberrant specimens

420   (Fig. 7 and Table 2). The species most commonly displaying aberrant forms are either *G. cretacea*

421   (14.4%) or *Ps. antecessor* (3.5%) for PFAS-1, and *Pv. longiapertura* (5.8%) for PFAS-2. The

aberrant specimens of PFAS-3α mainly belong to biserial taxa, especially to *Woodringina*

hornerstownensis (3.1%). The average aberrant index during PFAS-3α (6.6%) is significantly

lower than during PFAS-2 (11.5%), while during PFAS-3T1 it reaches 12.5%, which is similar

to that reached previously in PFAS-2. Triserial and biserial aberrant forms are dominant during

PFAS-3T substages, especially for *Chg. danica* and *W. hornerstownensis* species. During PFAS3-

T1, T2 and T3, aberrant forms of *Chg. danica* represent, respectively, 5.2, 1.6 and 0.3% on

average of total planktic foraminiferal specimens, and 3.3, 2.5 and 1.0% for *W. hornerstownensis*.

Each triserial bloom, i.e. PFAS-1, PFAS-3T1, PFAS3-T2 and to lesser extent PFAS3-T3, displays

a transient increase of the aberrant index (Fig 7 and Table 2). Conversely, during the blooming

episodes of the "other genera", i.e. PFAS-3O1, PFAS-3O2 and PFAS-3O3, there are fewer

aberrant specimens. The most common biserial species with aberrant forms within PFAS-3O

substages are *W. hornerstownensis* with respectively 1.8, 1.2 and 0.8% on average, and the most

common aberrant specimens of the "other genera" belong to the species *Globanomalina*

archeocompressa (0.55%) for PFAS3-O1, *Praemurica taurica* (0.4%) for PFAS3-O2 and *Pr.*

inconstans (0.3%) for PFAS3-O3.
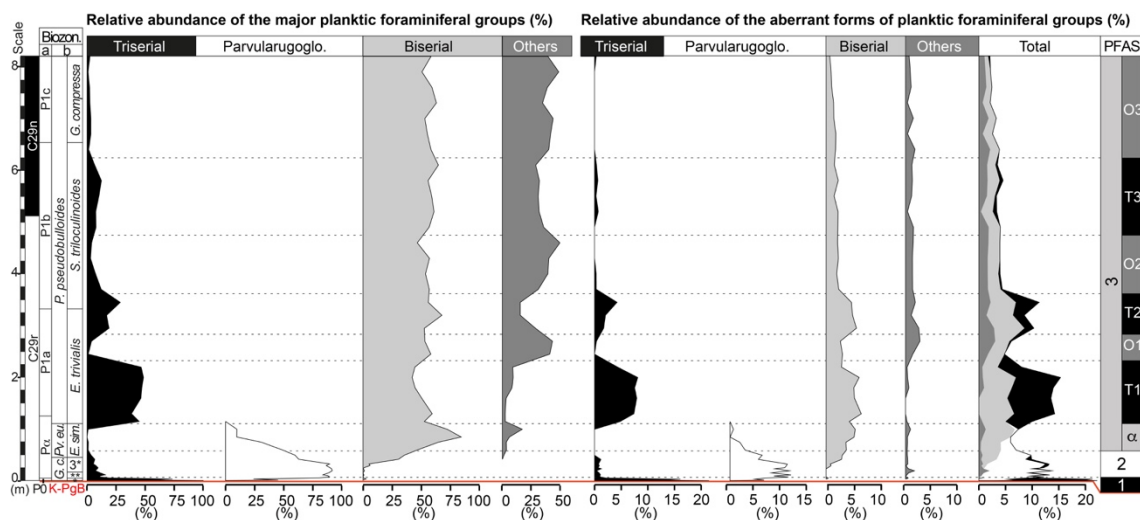
Fig. 7. Comparison of the quantitative results for the major groups of planktic foraminifera. Parvularugoglo.
= parvularugoglobigerinids.

3.6. Carbonate preservation and magnetic susceptibility

443

At Caravaca, the CaCO$_3$ content ranges from 15.5 to 88.4 % with a mean value of 73.78% (n = 70). The lowest CaCO$_3$ content has been identified in the K-PgB clay bed (0-6 cm, between 15.53 and 39.7%, and 28% on average). From 6 to 26 cm above the K-PgB, the CaCO$_3$ content increases sharply to 70%, and from 26 to 115 cm the average CaCO$_3$ content is 83%. There is a decrease in the average CaCO$_3$ content from 115 to 520 cm above the K-PgB (71%) with two relatively low values identified at 245 (60.5%) and 430 (65.5%) cm above the K-PgB (Fig. 8C). Finally, from 520 cm to the top of section, the average CaCO$_3$ content is relatively stable at 80% on average.

Apparent dissolution features on tests, such as abrasion marks, broken and/or isolated chambers, or corroded walls, have been identified, but they are not abundant. The planktic foraminiferal preservation is moderate to good in most of the samples, with the exception of those from the dark K-PgB clay bed. We consider that samples with planktic foraminiferal fragmentation ratio or fragmentation index (FI) >40% represent intervals of strong dissolution (e.g., Kucera et al., 1997; Gilabert et al., 2021). Values of planktic foraminiferal fragmentation vary between 7 and 45% across the Caravaca section, with an average fragmentation of 18.3% (n = 46). The average fragmentation values are high (45%) in the K-PgB dark clay bed, moderate (20%) between 6 and 520 cm, and low (13%) from 520 cm to the top of the section (Fig. 8D).

At Caravaca, the P/B ratio (Fig. 8F) ranges between 11 and 100%, with three distinct intervals: in the dark K-PgB clay bed P/B ratios range between 11 and 47%; from 6 to 26 cm above the K-PgB, they are between 72 and 89%; and from 30 cm to the top of the studied section, they are between 95 and 100%. Benthic foraminifera are more resistant to fragmentation and dissolution than planktic foraminifera, and the P/B ratio is expected to decrease with increasing dissolution intensity (Kucera et al., 1997). The significant, negative correlation r = -0.75 $p < 0.01$ between FI and the P/B suggests that higher dissolution of planktic foraminifera is related to lower P/B values, which are limited to the K-PgB clay bed.

Magnetic susceptibility (MS) oscillates between 1.67×10^{-8} and 1.23×10^{-7} m³/kg across the Caravaca section, with a mean value of 3.51×10^{-8} m³/kg. MS values are within the standard range of values for lithified marine samples containing typical paramagnetic minerals (Ellwood et al., 2008). MS values increase between 115 and 520 cm above the K-PgB, with maxima at 245 and 430 cm, mirroring the CaCO₃ curve (Figs. 8C and 8E). The strong negative correlation between MS and CaCO₃ content suggests variations in the original detrital influx or variations in the flux of carbonate, causing variations in the concentration of paramagnetic minerals.
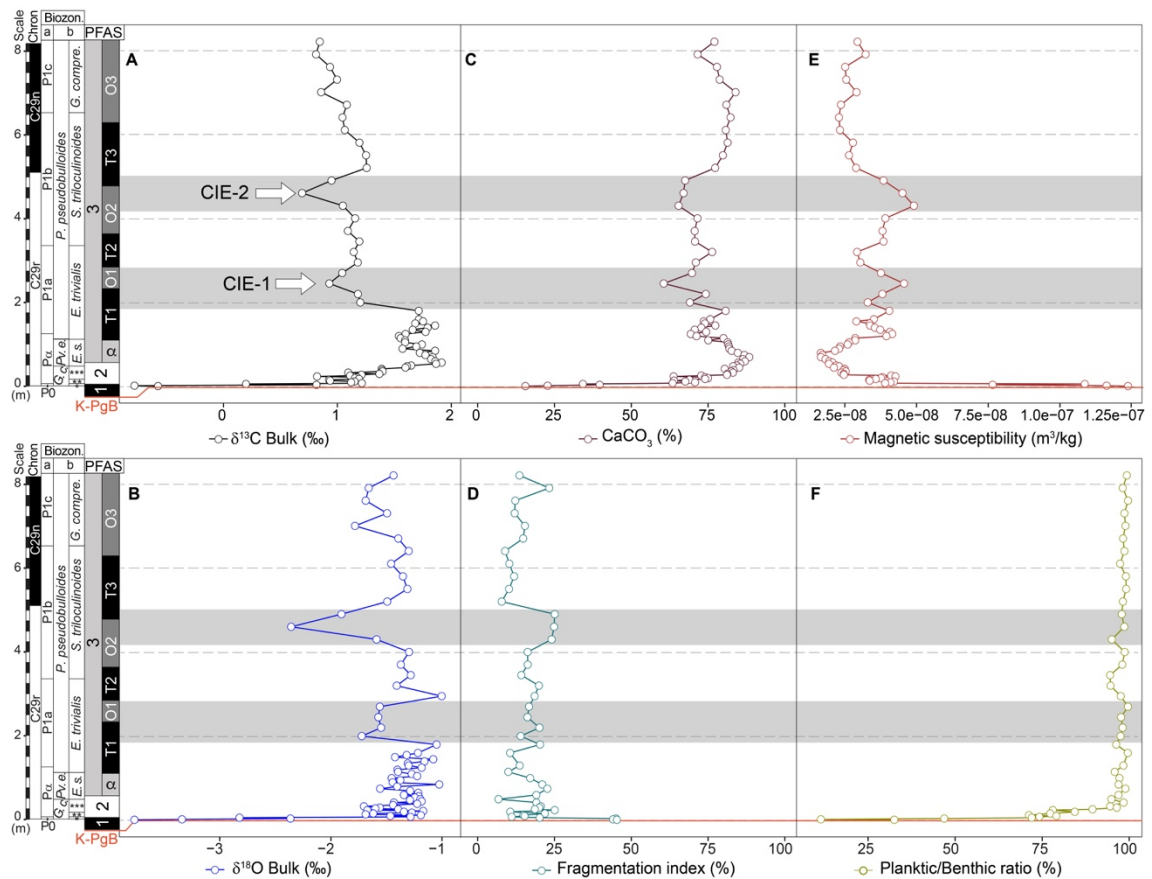
Fig. 8. A-B) Stable isotopes; C) Carbonate content; D) Fragmentation index; E) Magnetic susceptibility; and F) Planktic/Benthic ratio at Caravaca. Data can be found in Supplementary Table 4.

3.7. Stable isotopes (bulk carbonate δ¹³C and δ¹⁸O)

486 At Caravaca, $\delta^{13}C$ and $\delta^{18}O$ values for bulk carbonate show a moderate degree of correlation

487 (r = 0.62, p < 0.01) and evolve in parallel in some intervals. However, values are comparable with

488 those previously reported for the lower Danian at the Caravaca section (Kaiho et al., 1999; Sosa-

489 Montes de Oca et al., 2016; Sepúlveda et al., 2019) and other sections worldwide (see compilation

490 in Hull et al., 2020), suggesting little influence of diagenesis. Only in the K-PgB clay bed do

491 %$CaCO_3$ and stable isotope values exhibit a significant correlation. In the rest of the studied

492 section, the correlation between %$CaCO_3$ and $\delta^{18}O$ or $\delta^{13}C$ values is poor to very poor, with r =

493 0.54 (p < 0.01) between %$CaCO_3$ and $\delta^{13}C$, and r = 0.32 (p < 0.01) between %$CaCO_3$ and $\delta^{18}O$.

494 This lack of significant correlation suggests that the lithology exerts very little control on the

495 stable isotope values.

496

497 The $\delta^{13}C$ values vary between -0.78‰ and +1.92‰ at Caravaca (Fig. 8A) with the lowest

498 $\delta^{13}C$ values registered within the K-PgB dark clay bed, ranging from -0.78‰ to 0.20‰. From 6

499 to 57 cm above the K-PgB, $\delta^{13}C$ increases to the highest values of the section at ~1.92‰. Between

500 the maximum $\delta^{13}C$ value at 57 cm to 180 cm, $\delta^{13}C$ displays very small oscillations between 1.92

501 and 1.71‰. From 180 cm to the top of the section, $\delta^{13}C$ broadly displays a clear overarching trend

502 to lower values, with two negative carbon isotopic excursions (CIEs) superimposed upon this

503 trend. The first (CIE-1) has a minimum value of 0.93‰ at 245 cm and the second (CIE-2) a

504 minimum value of 0.69‰, at 460 cm above the K-PgB.

505

506 The $\delta^{18}O$ values are broadly invarient across much of the Caravaca section, except for three

507 distinct negative excursions (Fig. 8B), the first at the K-PgB and the other two coinciding

508 approximately with the CIEs described above. $\delta^{18}O$ values are the lowest of the whole section

509 within the K-PgB clay bed ranging from -3.77‰ to -2.82‰. The other two minima in $\delta^{18}O$ occur

510 at 200 cm above the K-PgB (slightly below the CIE-1), and 460 cm, coincident with CIE-2.

511

512 **4. Recognizing the Dan-C2 event at Caravaca**

513

514   The Dan-C2 event was first recognized in the NW Atlantic (ODP 1049), and SE Atlantic

515   (DSDP 527 and 528) and defined as a pair of major, fairly symmetrical, negative excursions in

516   δ^{13}C and δ^{18}O (Fig. 9), associated with decreased carbonate content and increased clay content

517   and magnetic susceptibility values (Quillévéré et al., 2008). At Caravaca, the stratigraphic interval

518   corresponding to Dan-C2, as defined in some Atlantic and Tethyan sections (Fig. 9), is recorded

519   between 200 and 490 cm above the K-PgB, from the middle part of *E.* cf. *trivialis* (P1a) Subzone

520   to the middle part of *S. triloculinoides* (P1b) Subzone, i.e. between 130 and 315 kyr after the K-

521   PgB according to our age model. The CIEs identified in Caravaca (CIE-1 and CIE-2) are within

522   this stratigraphic interval and consequently they are correlated with the two characteristic negative

523   excursions of Dan-C2 defined elsewhere (Quillévéré et al., 2008; Coccioni et al., 2010). Using

524   our age model, the peak minimum values of CIE-1 and CIE-2 occur 158 and 295 kyr, respectively,

525   after the K-PgB and each CIE has a duration of ~40 kyr. In addition, both CIEs are associated

526   with the lowest CaCO$_3$ content and the highest MS values. According to our age model, the entire

527   Dan-C2 event lasted approximately 185 kyr, ending around the C29r/C29n magnetic reversal

528   (Fig. 9 and Fig. 10A). The small discrepancies in the assigned ages of Dan-C2 between Caravaca

529   and elsewhere (Fig. 9) are probably related to differences and uncertainties in the age models

530   and/or variations in the local sedimentation rates between tie points that are not represented by

531   linear interpolation. Nevertheless, all of different records suggest a broadly consistent age for

532   Dan-C2 and a termination of the event near the C29r/C29n reversal.
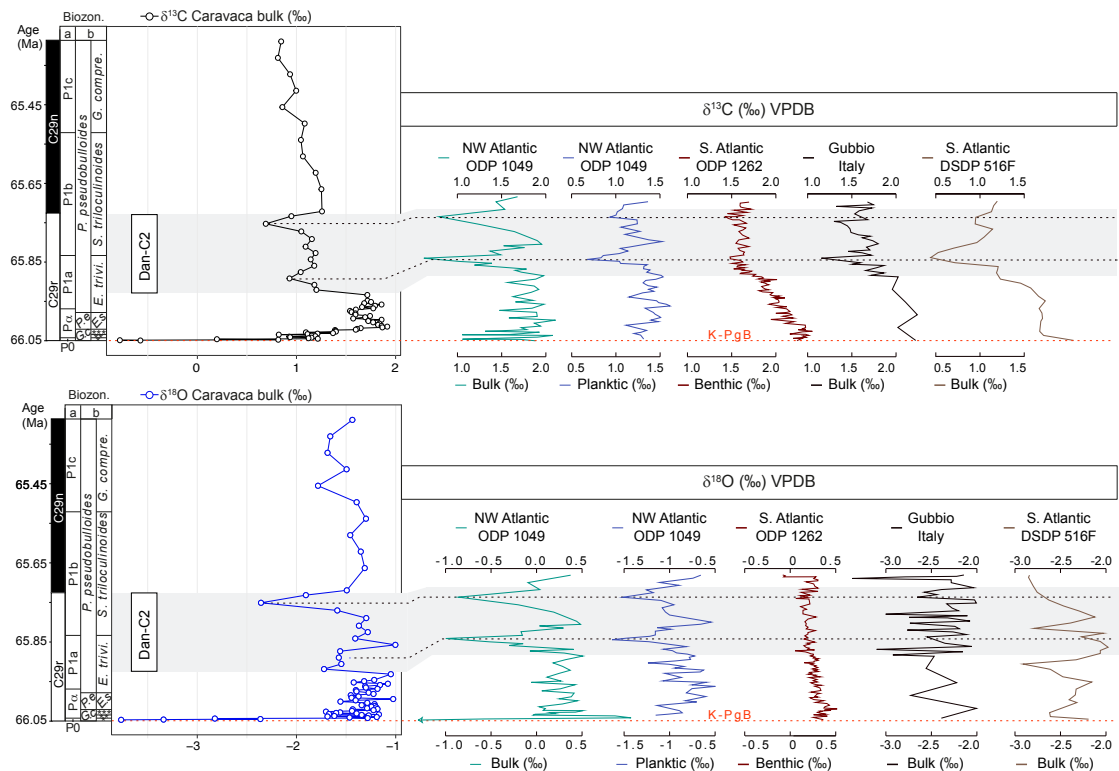
Fig. 9. Worldwide correlation of the Dan-C2 event according to our age model and the $\delta^{13}C$ and $\delta^{18}O$ records from several localities: Caravaca (this report), ODP Site 1049 (Quillévéré et al., 2008), DSDP Site 516 (Krahl et al., 2020), ODP Site 1262 (Barnet et al., 2019), and Contessa Highway (Gubbio) section (Coccioni et al., 2010).

5. Early Danian paleoenvironmental and paleoclimatic evolution

5.1. The K-PgB dark clay bed and PFAS-1 (Guembelitria acme): the aftermath of the Chicxulub impact

Worldwide, the K-PgB dark clay bed was deposited above the Chicxulub-linked air-fall layer under conditions of global climatic warming and alterations in oceanic productivity and acidity (D'Hondt et al. 1998; Coxall et al. 2006; Kawaragi et al., 2009; Birch et al. 2016; Henehan et al., 2016, 2019). At Caravaca, as in most continuous marine sections, the K-PgB dark clay bed is characterized by very low values in %CaCO$_3$, $\delta^{18}O$ and $\delta^{13}C$ (Figs. 8A, 8B and Figs. 10D, 10E) (see Schulte et al., 2010, and references therein). In addition, the highest planktic foraminiferal

550   fragmentation index values at Caravaca occur within the K-PgB dark clay bed. These geochemical

551   and preservational changes have been directly related to the decimation of pelagic marine

552   calcifiers at the K-PgB (Smit, 1982; Bown, 2005), and subsequent ocean acidification (Alegret et

553   al., 2012; Henehan et al., 2019). At Caravaca, the P/B ratio across the K-PgB dark clay bed is

554   very low, around 30% in comparison to the P/B ratio values-for most of the Danian (Table S2).

555   This decreased P/B ratio is more compatible with the sudden extinction of planktic foraminifera

556   at the K-PgB than with rapid paleobathymetric changes, as previously shown by Alegret et al.

557   (2003). Therefore, the K-PgB dark clay bed records a brief interval of time in which the

558   ecosystems collapsed and the oceans acidified (D´Hondt et al., 1998; Arenillas et al., 2006, 2018;

559   Kring, 2007; Henehan et al., 2019). Biological recovery, however, was relatively quick and

560   oceanic productivity was rapidly re-established after the K-PgB (Sepúlveda et al., 2009, 2019;

561   Lowery et al., 2018; Gibbs et al., 2020). Productivity may have been controlled by blooms in the

562   non-calcareous algal and microbial communities in the open ocean after the K-PgB event, which

563   potentially provided a food supply for higher trophic levels such as calcareous plankton (Bralower

564   et al., 2020).

565

566   The acme of the stress tolerant and opportunistic genus *Guembelitria* during PFAS-1 is

567   recorded within the K-PgB dark clay bed, immediately above the air-fall layer.

568   Contemporaneously, the start of an acme of the opportunist calcareous dinocyst *Thoracosphaera*

569   (Fig. 10B) has been reported above the K-PgB at Caravaca (Lamolda et al., 2005, 2016) and in

570   many other Tethyan sections (Romein, 1977; Smit, 1982; Pospichal, 1996; Gardin, 2002;

571   Lamolda et al., 2005, 2016; Fornaciari et al., 2007; Thibault et al., 2018). The highest planktic

572   foraminiferal aberrant index (21%) of the whole section occurs in PFAS-1 (Fig. 10C); a value

573   which is comparable to other Tethyan and North Pacific localities (Gerstel et al., 1986; Coccioni

574   and Luciani, 2006; Arenillas et al., 2018), suggesting stressed conditions on a global scale.

575   Detrimental environmental effects such as eutrophication, warming, ocean acidification, low

576   oxygenation, and the remobilization of pollutants and toxic heavy metals all occurred potentially

577   in the aftermath of Chicxulub impact and can be attributed to it (Smit, 1999; Coccioni and Luciani,

578   2006; Ballent and Carignano, 2008; Omaña et al., 2012; Arenillas et al., 2018; Henehan et al.,

579   2019). Nonetheless, a minor contribution by Deccan volcanism to some of these environmental

580   changes cannot be entirely ruled out.

581

582   *5.2. PFAS-2: recovery and the first radiation of planktic foraminifera*

583

584   Within PFAS-2, an initial recovery of planktic foraminiferal assemblages and a first

585   evolutionary radiation took place. This first evolutionary radiation was mostly related to the

586   evolution and proliferation of the tiny trochospiral species belonging to *Parvularugoglobigerina*

587   and *Palaeoglobigerina* genera. Recently, Arenillas and Arz (2017) proposed that

588   parvularugoglobigerinids originated from a benthic foraminifer that evolved into a planktic form,

589   such as *Ps. antecessor*. Both *Parvularugoglobigerina* and *Palaeoglobigerina* genera radiated and

590   proliferated during PFAS-2, which, together with the continued dominance of *Thoracosphaera*

591   (Lamolda et al., 2005, 2016) and the very high (11.5%) abundance of aberrant specimens,

592   suggests that conditions remained unstable and stressed throughout PFAS-2.

593

594   At Caravaca, a rapid rebound (< 20 kyr) of the carbonate preservation state between PFAS-

595   1 and PFAS-2 is supported by the rapid increase in %$CaCO_3$ and P/B ratios, and a decrease in the

596   fragmentation index and MS values (Fig. 8). According to Henehan et al. (2016, 2019), the initial

597   surface ocean acidification after the K-PgB, together with the extinction of calcifying organisms,

598   would have led to a transient reduction in the marine alkalinity sink. With the return of marine

599   calcifiers, the excess of alkalinity in seawater was removed leading to a rapid rebound and

600   overshoot in surface ocean pH within 40 kyr after the K-PgB. This process likely explains the

601   rapid increase in %$CaCO_3$ during PFAS-2. The $\delta^{13}C$ values sharply increase through PFAS-2,

602   returning to relatively stable background values similar to those recorded in the uppermost

603   Maastrichtian of Caravaca (e.g. Kaiho et al.,1999; Sosa-Montes de Oca et al., 2016; Gilabert et

604   al., 2021). This trend in $\delta^{13}C$ also suggests that there was a rapid return of oceanic productivity

605   (Sepúlveda et al., 2019).

607 *5.3. Onset of PFAS-3* (PFAS-3α) *and the second radiation of planktic foraminifera*

608

609   The biserial taxa *Woodringina* and *Chiloguembelina* proliferated throughout PFAS-3 but

610   especially during PFAS-3α, when *Woodringina* was the dominant taxon (Fig. 5). A second

611   radiation of Danian planktic foraminifera took place within PFAS-3α with the first appearance of

612   several incoming Danian genera including *Eoglobigerina*, *Globanomalina*, *Parasubbotina*,

613   *Praemurica* and *Trochoguembelitria*. Most of these new genera seem to have occupied

614   thermocline and subthermocline depths (see Olsson et al., 1999; Aze et al., 2011 and references

615   therein) thus suggesting an initial reoccupation of deeper depth habitats and an incipient but

616   increased water column stratification. The dominance of *Woodringina* during PFAS-3α suggests

617   relatively warm conditions (see Olsson et al., 1999 and references therein) during this stage. A

618   similar bloom of biserial taxa at Gubbio has been interpreted as an overall reduction in

619   oxygenation of the mixed layer in the oceans (Coccioni et al., 2010) similar to conditions during

620   blooms of biserial taxa during the late Maastrichtian (Pardo and Keller, 2008).

621

622   During PFAS-3α, *Thoracosphaera* was still the dominant calcareous nannoplankton genera

623   although *Braarudosphaera* started to replace it as the dominant taxon, at least in the western

624   Tethys (Romein 1977; Smit, 1982; Lamolda et al., 2016). *Braarudosphaera* species are thought

625   to have been abundant in the lower photic zone under low temperature, low salinity, and eutrophic

626   conditions, and therefore *Braarudosphaera* species are typically considered opportunists and are

627   associated with episodes of environmental stress (Bukry, 1974; Cunha and Shimabukuro, 1997;

628   Kelly et al., 2003; Lamolda et al., 2005, 2016; Jones et al., 2019). The appearance of incoming

629   species of planktic foraminifera and nannofossils characteristic of deeper water depth habitats

630   suggests a first step for the recolonization of deeper niches. However, it is well-known that the

631   entire reoccupation of the deeper ocean niches by planktic foraminifera, as well as the rebound of

632   diversity levels comparable to pre-KBP levels, took several million years (Aze et al., 2011; Birch

633　et al., 2012, 2016; Lowery and Fraas, 2019). Within PFAS-3α, carbonate parameters (%CaCO$_3$

634　and the fragmentation index) are similar to those in PFAS-2.

635

636　*5.4. Chiloguembelitria blooms during PFAS-3 and the Dan-C2 event*

637

638　　　Triserial guembelitriid blooms like those recorded during PFAS-3T substages are the most

639　common planktic foraminiferal indicators of high environmental stress (Kroon and Nederbragt

640　1990; Coccioni and Luciani, 2006; Pardo and Keller, 2008; Punekar et al., 2014a,b; Arenillas et

641　al., 2018). In addition, during each triserial bloom identified at Caravaca, a rise in the aberrant

642　index has been identified (Fig. 10B and 10C). Danian triserial guembelitriid blooms have been

643　commonly ascribed to the effect of Deccan volcanism, and linked to the Dan-C2 event (Punekar

644　et al., 2014a; Keller et al., 2016). At Caravaca, the two main *Chiloguembelitria* blooms (PFAS-

645　3T1 and T2) are related to strong increases in the aberrant index (Fig. 7), suggesting higher stress

646　conditions, similar to those reported in Tunisian sections (Arenillas et al., 2018).

647

648　　　A triserial guembelitriid acme, such as the bloom of *Guembelitria* (here *Chiloguembelitria*)

649　during PFAS-3T1, has frequently been reported at other Tethyan localities (Arenillas et al., 2000a,

650　b, 2018; Keller, 2003; Coccioni et al., 2010; Punekar et al., 2014a,b), always above the onset of

651　the biserial acme of PFAS-3 (here PFAS-3α). In addition, this acme has been reported in the Gulf

652　of Mexico (Arz et al., 2001; Abramovich et al., 2011), in the North Pacific (Smit and Romein,

653　1985), in the Western North Atlantic (Mateo et al., 2016), and in the Parathetys (Punekar et al.,

654　2016). Therefore, PFAS-3T1 probably characterizes a global response to environmental stress.

655

656　　　During PFAS3T-1, the low-oxygenated sub-thermocline dweller *Chiloguembelina* (Boersma

657　and Premoli Silva, 1989; Olsson et al., 1999; Aze et al., 2011; Luciani et al., 2020) became more

658　abundant than during PFAS-3α, suggesting the progressive reoccupation of the deeper-most

659　niches initiated in PFAS-3α. *Chiloguembelina* stabilized in abundance through the section (Fig.

660 5 and Fig. 10B) suggesting that the oxygen minimum zone did not show major changes during

661 the studied interval. Nevertheless, near the end of PFAS3-T1 (around the onset of Dan-C2), the

662 *Braarudosphaera* bloom was followed by an acme of *Neobiscutum* species (Fig. 10B; Romein,

663 1977; Gardin and Monechi, 1998, Gardin, 2002; Lamolda et al., 2016; Thibault et al., 2018),

664 suggesting rapidly changing ecological conditions in the upper part of the water column during

665 the beginning of the Dan-C2 event.

666

667 Conversely to what may be expected, the minima of both Dan-C2 CIEs occurred during

668 PFAS-3O substages instead of during triserial blooms. This lack of coincidence between the

669 evidence for C-cycle perturbation and biotic stress was also noted in Italy (Coccioni et al., 2010)

670 and can also be observed in the data reported by Punekar et al. (2014a) from Israel, Egypt and the

671 USA. Since bulk $\delta^{18}O$ and $\delta^{13}C$ mostly reflect changes in the upper part of the water column it

672 can be assumed that transient surface water warming occurred during both CIEs. No evidence of

673 bottom water warming has been detected in the Dan-C2 interval, based on benthic foraminiferal

674 $\delta^{18}O$ (Fig. 9; see Barnet et al., 2019 and references therein). Instead, the warming indicated by

675 the bulk oxygen isotope data may have led to a rapid thermal stratification of the upper part of

676 the water column that caused a stronger thermal gradient between the near-surface waters and the

677 thermocline, creating more differentiated ecological niches. The increase of the deeper water

678 dwelling species (such as *Chiloguembelina*, *Eoglobigerina*, *Globanomalina* and *Parasubbotina*)

679 during both CIEs agrees with transient but enhanced ocean stratification (Fig. 5 and Figs. 10B,

680 10E). The overall planktic foraminiferal assemblage response during Dan-C2 interval is

681 represented by an alternation between the triserial blooms (PFAS-3T1, 2, 3) and increases in other

682 genera (PFAS3-O1, 2) which are progressively less abrupt through time (Fig. 8 and Fig. 10B).

683 These ecological alternations suggest rapidly changing conditions but also a slightly more

684 resilient and stable ocean, compared to the very earliest Danian. During the Dan-C2 event, $CaCO_3$

685 dissolution due to ocean acidification has been invoked (see Coccioni et al., 2010; Krahl et al.,

686 2020 and references therein) but, at Caravaca, the dissolution-sensitive parameters (fragmentation

687 index, $CaCO_3$ content and P/B ratio) do not show evidence of strong dissolution, although we

688   note that there are slight decreases in the %CaCO$_3$ content and slight increases in the

689   fragmentation index within the Dan-C2 interval, roughly coincident with the two CIEs.

690

691   *5.5. End of PFAS-3: Shift to a more stable ocean*

692

693   The stabilization of the planktic foraminiferal assemblages at Caravaca seems to have been

694   completed in PFAS-3O3, although there are some differences in comparison to the previous

695   PFAS-3O substages. During PFAS-3O3, *Praemurica* significantly increases in abundance, and

696   the triserial *Chiloguembelitria* is replaced by the trochospiral guembelitriid *Globoconusa* (Fig. 5,

697   Fig. 10B and Table S2). The combined abundances of the *Chiloguembelitria* and *Globoconusa*

698   genera is lower than the abundance reached by *Chiloguembelitria* in any of the preceding acme

699   stages and substages, suggesting lower environmental stress conditions from PFAS-3O3 onwards.

700

701   During PFAS-3O3 newly incoming nannoplankton taxa become dominant, including the r-

702   selected opportunist *Futyana petalosa* and the first K-strategists *Cruciplacolithus* and

703   *Coccolithius* (Romein, 1977; Gardin, 2002; Thibault et al., 2018; Jiang et al., 2019).

704   *Cruciplacolithus* and *Coccolithius* are generally reported as oligotrophic taxa (Jiang et al., 2010,

705   2019), suggesting that the upper ocean waters at Caravaca became more oligotrophic during

706   PFAS-3O3. Oligotrophic conditions at Caravaca are also supported by the very low abundance

707   of *Chiloguembelitria* and by the rise of the *Praemurica* lineage, within which planktic

708   foraminifera species first acquire symbionts during the Paleocene (Norris, 1996; Birch et al.,

709   2012). In addition, carbonate content, magnetic susceptibility, fragmentation index, the P/B ratio

710   and isotopic proxies show only minor oscillations in PFAS-3O3, suggesting relatively stable

711   conditions (Fig. 8).
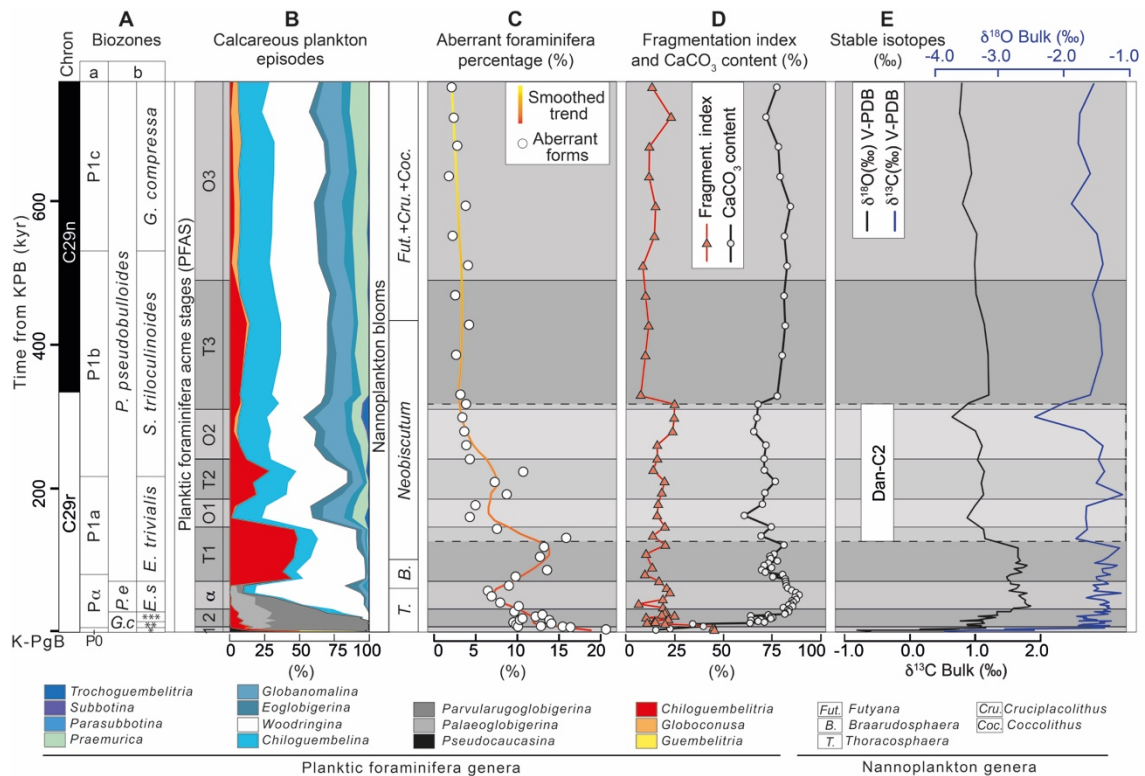
Fig. 10. Synthesis of the results obtained in this study: A) Planktic foraminiferal biozonations: a = Wade et al. (2011); b = Arenillas et al. (2004); B) Relative abundances of Danian planktic foraminiferal genera, and correlation of the planktic foraminiferal acme-stages (PFAS) and calcareous nannoplankton blooms (see references in the text); C) Relative abundance of planktic foraminiferal aberrant specimens; D) Main carbonate sensitivity parameters; E) Bulk carbonate stable isotopes.

6. What was the environmental impact of the Deccan Traps during the earliest Danian?

For several decades, identifying the role of the Deccan Traps (India) in environmental and climatic change across the K-PgB has been difficult, mainly due to the uncertainties associated with radioisotopic dating (e.g., Courtillot et al., 1986; Vandamme et al., 1991; Chenet et al., 2007). However, recent improvements in radiometric methods have led to refined estimates of the duration of Deccan volcanism, at less than 1 Myr (Schoene et al., 2019; Sprain et al., 2019), and allowed for a more robust correlation between volcanism and climate change (e.g., Barnet et al., 2018; Hernandez Nava et al., 2021). Whether the major eruptive episodes of the Deccan Traps occurred before or after the K-PgB remains a topic of intense debate, since the timing has

729   profound implications for the role of the Deccan Traps in the K-PgB mass extinction (Burgess,

730   2019; Hull et al., 2020; Keller et al., 2020). This controversy over the role of volcanism in the

731   extinction event is mostly related to uncertainty over the stratigraphic position of the K-PgB

732   within the Deccan Traps sequence.

733

734   Based on ^{40}Ar/^{39}Ar dating, Sprain et al. (2018) reported an age of $66.052 \pm 0.008/0.043$ for

735   the K-PgB, supporting the hypothesis that the most voluminous formations of the Deccan Traps,

736   which belong to the Wai subgroup (Poladpur, Ambenali and Mahabaleswar), are placed above

737   the K-PgB (Jay and Widdowson, 2008; Renne et al., 2015; Richards et al., 2015; Sprain et al.,

738   2019). According to the eruptive model of Sprain et al. (2019), the K-PgB is near the base of the

739   Poladpur Formation, and thus the most voluminous eruptive episodes of the Deccan Traps may

740   be early Danian in age. However, based on U-Pb dating, Clyde et al. (2016) reported an age of

741     $66.021 \pm 0.24/0.039$ Ma for the K-PgB, supporting the emplacement of the Poladpur Formation

742   prior to the K-PgB (Schoene et al., 2015, 2019, 2021; Kasbohm et al., 2021; Fig. 11). According

743   to the eruptive model of Schoene et al. (2019), the emplacement of the Poladpur Formation,

744   (which achieved the highest eruption rate of Deccan volcanism) occurred in the latest

745   Maastrichtian, preceding the K-PgB by only some tens of thousands of years. Schoene et al.

746   (2021) recalculated the eruptive volumes of the model of Sprain et al. (2019) in terms of eruptive

747   rate (Fig. 11), which clearly distinguishes between the mega-pulse eruptive model of Schoene et

748   al. (2019) and the quasi-continuous eruptive model of Sprain et al. (2019).

749
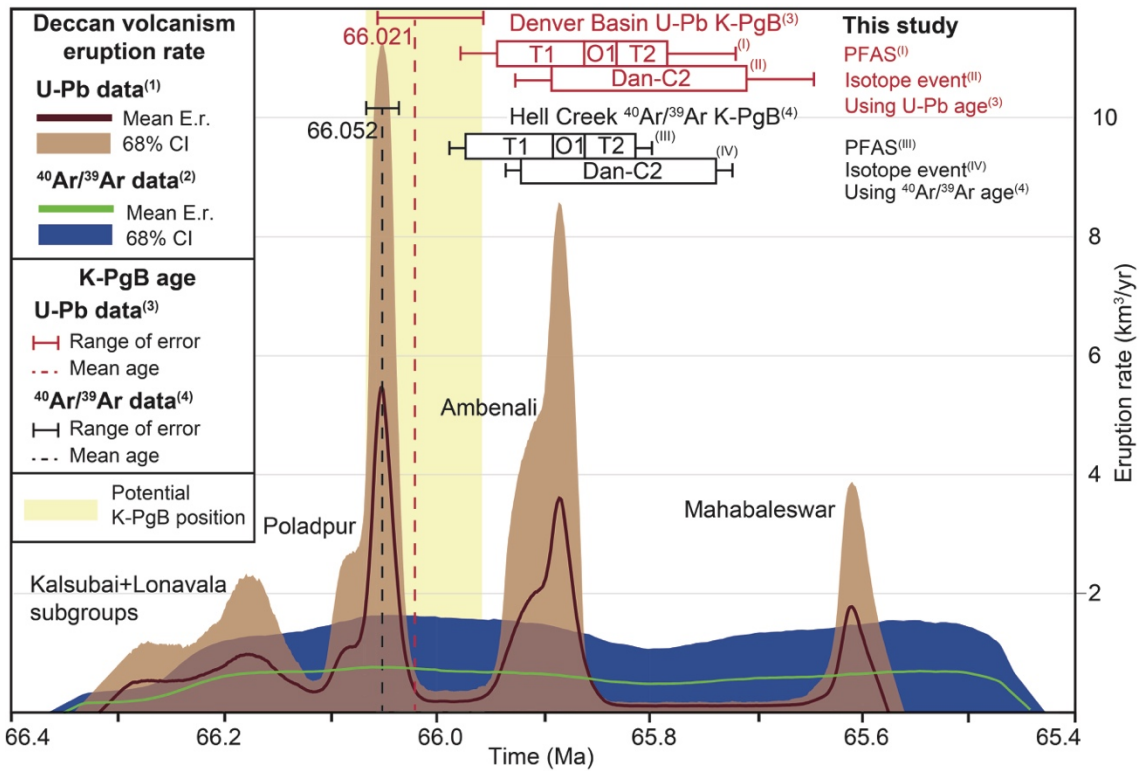
Fig. 11. Age models and eruption rates for the Deccan Traps based on Fig. 4 of Schoene et al. (2021), compared with the age of key early Danian paleontological and climatic events as determined in the Caravaca section. The yellow band shows the most probable stratigraphic range for the K-PgB position within the Deccan Traps, considering both the range of error on U-Pb and ^{40}Ar/^{39}Ar dates. Our preferred age model for Caravaca is anchored at the K-PgB using an ^{40}Ar/^{39}Ar age of 66.052 Ma, but we also show how the relationship between Deccan volcanism and the PFAS-3T1, 3O1 and 3T2 and Dan-C2 events could vary by changing the age of the K-PgB to that derived from U-Pb (66.021 Ma). Error margins for both radiometric techniques are also shown and incorporated into the age estimates of early Danian events. E.r. = eruption rate; CI =Confidence interval (1) = (Schoene et al., 2019); (2) = (Sprain et al., 2019); (3) = (Clyde et al., 2016); (4) = (Sprain et al., 2018).

The Rajahmundry Traps (RT, SE India) bear witness to the scale of early Danian Deccan volcanism, extending ~1000 km from the erupting center and forming the longest lava flows on Earth (Self et al., 2008; Keller et al., 2011, 2012). The exposed flows of the RT have been dated as early Danian in age (Keller et al., 2008; Fendley et al., 2020) and have been geochemically assigned to the Ambenali and Mahabaleshwar Formations in the Western Ghats (Baksi, 2001; Self et al., 2008). The age of the RT is also compatible with the recently published radiometric

768   ages of the Ambenali and Mahabaleshwar Formations (Schoene et al., 2019; Sprain et al., 2019).

769   However, the eruption and outgassing rates in each phase of Deccan volcanism are considered

770   potentially more important for climate change than the volume of basalt erupted (Self et al., 2006;

771   Gertsch et al., 2011; Hernandez Nava et al., 2021). Recent estimations of the amount and rates of

772   CO_2 release from Deccan volcanism predict only minor increases in atmospheric CO_2 compared

773   to the background Cretaceous–Paleogene atmospheric reservoir (Self et al., 2006; Schmidt et al.,

774   2016; Steinthorsdottir et al., 2016; Henehan et al., 2016; Fendley et al., 2020). Modelling of

775   different climate sensitivities and volcanic outgassing scenarios suggest that Deccan volcanism

776   alone was insufficient to have driven warming during the early Danian (Hull et al., 2020; Fendley

777   et al., 2020). Conversely, the influence of volcanic SO_2 and halogen emissions could have been

778   profound at times of flood basalt emplacement (Self et al., 2006). Although volcanic aerosols

779   have a short residence time in the troposphere of ∼1 week, flood basalt activity could have

780   provided a semi-continuous SO_2 supply (Self et al., 2006), which may have resulted in cooling

781   and/or ocean acidification on geologic time scales (Gertsch et al., 2011; Courtillot and Fluteau,

782   2014).

783

784   Our data show no indications of ocean acidification or temperature changes in the first 50

785   kyr of the Danian, except within the K-PgB clay bed, and thus the effect of volcanic outgassing

786   directly following the Chicxulub impact (Renne et al., 2015; Sprain et al., 2019) may have been

787   obscured by the extinction of calcifying plankton (Henehan et al., 2019). Alternatively, our data

788   could indicate that there was no significant Deccan volcanic activity during the earliest Danian.

789   This would be in accordance with Schoene et al. (2019), who suggested that the Poladpur eruptive

790   pulse occurred in the latest Maastrichtian and was followed by a period of volcanic inactivity in

791   the Deccan for about 100 kyr, extending into the earliest Danian. The return to higher stressed

792   environmental conditions at Caravaca occurred ~70 kyr after the K-PgB, as evidenced by the

793   *Chiloguembelitria* bloom in PFAS-3T1, which is broadly coincident with the eruption of the

794   Ambenali Formation (Schoene et al., 2019; Sprain et al., 2019). Recent pH estimates, based on

795   boron isotopes, show initial surface water acidification after the K-PgB, followed by a rapid

796   rebound and overshoot in surface ocean pH within 40 kyr, before pH values returned to pre-K-

797   PgB background levels after ~120 kyr (Henehan et al., 2019). Previous ocean pH estimates

798   predicted a rise in pH due to the extinction of calcifying organisms and the consequent transient

799   reduction in the marine alkalinity sink (Caldeira et al., 1990; Henehan et al., 2016). The latter is

800   supported by observations of improved deep-sea carbonate preservation during the time of the pH

801   overshoot (e.g. Minoletti et al., 2005; Alegret and Thomas, 2013; Tobin et al., 2017) and by our

802   own data (see section 5.1 and 5.2).

803

804   At Caravaca, the aberrant index follows a declining trend during the first ~70 kyr of the

805   Danian, from PFAS-1 to PFAS-3α, suggesting a reduction in the impact of the different

806   environmental stressors with a rapid recovery of productivity. Conversely, during the following

807   ~80 kyr (in PFAS-3T1), the opportunistic *Chiloguembelitria* bloomed at a global scale, and the

808   aberrant index increased again (see section 5.4), suggesting a new episode of environmental

809   stress. Commonly, guembelitriid blooms are reported from shallow marine areas, often near

810   volcanic provinces with a high nutrient flux (Pardo and Keller, 2008). However, these

811   opportunistic taxa radiated and proliferated in the pelagic realm after the K-PgB (Olsson et al.,

812   1999; Arenillas et al., 2000a,b; Keller, 2003), suggesting that, during the early Danian, their

813   ecological preferences of high nutrient availability were met in the open ocean. Although the

814   uncertainties in the temporal correlation between Deccan Traps volcanic phases, the K-PgB, and

815   climatic and paleobiological events are still significant, our data suggest that the

816   *Chiloguembelitria* bloom (PFAS-3T1) is coeval with the emplacement of the Ambenali

817   Formation (Fig. 11).

818

819   The emplacement of the Ambenali formation and the apparent co-occurrence with the Dan-

820   C2 event in the upper part of C29r (Fig. 10A and 10D), has led some authors to link these two

821   events mechanistically (Coccioni et al., 2010; Krahl et al., 2020; Punekar et al., 2014a). However,

822   the Dan-C2 event was not associated with bottom water warming (Quillévéré et al., 2008;

823   Coccioni et al., 2010; Barnet et al., 2019; Krahl et al., 2020) which raises questions as to whether

824 this event can be considered a 'true' hyperthermal event or not (see discussion in Barnet et al.,

825 2019). Ocean acidification has also been invoked during Dan-C2 (Coccioni et al., 2010; Krahl et

826 al., 2020) but no convincing evidence has been identified during the Dan-C2 interval at Caravaca

827 nor in other sections to support this (see Barnet et al., 2019). The exact mechanisms that drove

828 the Dan-C2 event are poorly resolved, and several hypotheses have been put forward: pulses of

829 massive Deccan volcanic eruptions (Krahl et al., 2020); a combination of Deccan volcanism with

830 an orbital configuration which perturbed the carbon cycle (e.g. Coccioni et al., 2010; Barnet et

831 al., 2019; Sinnesael et al., 2019); and/or passive degassing of CO_2 due to the interaction of

832 intrusive magma bodies with the crust (see Sprain et al., 2019; Fendley et al., 2020). The quasi-

833 continuous eruptive model suggests that the Ambenali Formation represents a relatively long

834 volcanic episode (Renne et al., 2015; Sprain et al., 2019). Although this scenario does not provide

835 a relatively rapid trigger mechanism for environmental change, it still permits a hypothesis that

836 the Deccan volcanism could add to emissions of CO_2 by passive degassing over longer timescales,

837 contributing, albeit perhaps in a minor way, to early Danian climate change and the Dan-C2 event.

838 Conversely, the hypothesis of a shorter (<100 kyr), more intense, volcanic pulse (Schoene et al.,

839 2019) is not supported by geochemical evidence from marine records (Hull et al., 2020), and

840 would imply a minimal impact of volcanic activity on climate. Regardless of the eruptive model

841 favoured, and considering the estimated duration for the Ambelani eruptive episode, volcanic

842 outgassing from the Deccan Traps by itself was probably insufficient to drive significant warming

843 during the early Danian (Fendley et al., 2020; Hull et al., 2020), although it may have exacerbated

844 environmental stress. Our age model allows us to suggest that the Ambenali phase coincided with

845 the first Dan-C2 CIE, but not with the second CIE (Fig. 11). If Deccan volcanism was not the

846 cause of the second CIE, then it seems that other factors, such as orbital forcing, are required to

847 fully explain the Dan-C2 event.

848

849 Since the proposed warming for the Dan-C2 event is only observed in bulk and planktic

850 foraminiferal isotopic records (Fig. 9), the increase in temperature probably only affected surface

851 ocean waters. A transient but enhanced thermal stratification of the upper part of the water column

852   may have resulted in more differentiated ecological niches. This is supported by our data at

853   Caravaca, which show rapid turnovers of planktic foraminiferal assemblages in PFAS-3O1 and

854   O2 coinciding approximately with both Dan-C2 CIEs. Remarkably, continental records of the

855   first ~700 kyr of the Danian have documented increases in ecologic diversification of plants and

856   mammals (suggested by increased species richness and taxonomic composition), coinciding with

857   the warmer intervals of the early Danian (Lyson et al., 2019; Chiarenza et al., 2020). Therefore,

858   if the Dan-C2 event influenced both marine and terrestrial ecosystems (driven by Deccan

859   volcanism, orbital forcing, or a combination of those and additional mechanisms), it did not cause

860   harmful environmental effects, but instead may have temporarily boosted the recovery of

861   ecosystems.

862

863   **6. Conclusions**

864

865   High-resolution planktic foraminiferal, geochemical and paleomagnetic analyses of the first

866   ~750 kyr of the Danian at Caravaca (Spain, western Tethys) were carried out. Planktic

867   foraminiferal assemblages after the Cretaceous-Paleogene boundary (K-PgB) are characterized

868   by a rapid succession of planktic foraminiferal acme-stages (PFAS). The first acme is of the

869   triserial *Guembelitria* (PFAS-1), the second of the tiny trochospiral *Parvularugoglobigerina-*

870   *Palaeoglobigerina* (PFAS-2), and the third of the biserial *Woodringina-Chiloguembelina* (PFAS-

871   3). Within PFAS-3, seven shorter substages are distinguished: PFAS-3α during the maximal

872   bloom of biserials, PFAS-3T1, T2 and T3 for blooms of the triserial *Chiloguembelitria*, and

873   PFAS-3O1, O2, O3 for increases in abundance of the trochospiral genera *Eoglobigerina*,

874   *Praemurica*, *Globanomalina* and *Parasubbotina*. Triserial blooms and a high abundance of

875   aberrant forms are striking evidence of enhanced environmental stress, occurring especially

876   within PFAS-1 and PFAS-3T substages, during the first 230 kyr of the Danian.

877

878   On the basis of $\delta^{18}O$ and $\delta^{13}C$, $CaCO_3$ content and magnetic susceptibility, the Dan-C2 event

879   has been identified for the first time at the Caravaca section. The two carbon isotopic excursions

880 (CIEs) that characterize the Dan-C2 event have been linked to surface water warming that caused

881 enhanced thermal stratification. During both CIEs, the PFAS-3T assemblages were rapidly

882 replaced by the PFAS-3O assemblages containing less opportunistic taxa, probably because the

883 water depth habitats became more differentiated. High carbonate dissolution is restricted to the

884 K-PgB clay bed, while the Dan-C2 event and the rest of the section show no evidence of

885 significant carbonate dissolution episodes. Although there are still uncertainties in radiometric

886 dating, our data suggest that the first and largest *Chiloguembelitria* bloom (PFAS-3T1) coincided

887 with the emplacement of the Ambenali Formation of the Deccan Traps. Conversely, the Dan-C2

888 event was decoupled from both the Ambenali eruptive pulse and the *Chiloguembelitria* bloom,

889 starting long after these events had occurred. This suggests that volcanic outgassing of CO_2 was

890 insufficient to drive warming, which only occurred only when the effects of volcanic CO_2 were

891 combined with other factors such as a specific orbital configuration. More high-resolution

892 multidisciplinary studies are needed to fully assess the relationship between Deccan Traps

893 volcanism on early Danian climate, and its potential contribution in reshaping life on Earth after

894 the end-Cretaceous mass extinction.

895

896 **Acknowledgements**

897

904

905 **References**

906   Abramovich, S., Keller, G., Berner, Z., Cymbalista, M., Rak, C., 2011. Maastrichtian Planktic

907   Foraminiferal Biostratigraphy and Paleoenvironment of Brazos River, Falls County,

908   Texas, U.S.A., in: Keller, G., Adatte, T. (Eds.), The End-Cretaceous Mass Extinction and

909   the Chicxulub Impact in Texas. SEPM (Society for Sedimentary Geology), Tulsa, pp. 123-

910   156. https://doi.org/10.2110/sepmsp.100.123.

911   Alegret, L., Thomas, E., 2013. Benthic foraminifera across the Cretaceous/Paleogene boundary

912   in the Southern Ocean (ODP Site 690): Diversity, food and carbonate saturation. Mar.

913   Micropaleontol. 105, 40-51. https://doi.org/10.1016/j.marmicro.2013.10.003.

914   Alegret, L., Molina, E., Thomas, E., 2003. Benthic foraminiferal turnover across the

915   Cretaceous/Paleogene boundary at Agost (southeastern Spain): Paleoenvironmental

916   inferences. Mar. Micropaleontol. 48, 251-279. https://doi.org/10.1016/S0377-

917   8398(03)00022-7.

918   Alegret, L., Thomas, E., Lohmann, K.C., 2012. End-Cretaceous marine mass extinction not

919   caused by productivity collapse. Proc. Natl. Acad. Sci. USA 109, 728-732.

920   https://doi.org/10.1073/pnas.1110601109.

921   Alvarez, L.W., Alvarez, W., Asaro, F., Michel, H. V., 1980. Extraterrestrial cause for the

922   Cretaceous-Tertiary extinction. Science 208, 1095-1108.

923   https://doi.org/10.1126/science.208.4448.1095.

924   Andeweg, B., 2002. Cenozoic tectonic evolution of the Iberian Peninsula: effects and causes of

925   changing stress fields. PhD thesis, Vrije Universiteit Amsterdam, Amsterdam, 192 pp.

926   Arenillas, I., Arz, J.A., 2017. Benthic origin and earliest evolution of the first planktonic

927   foraminifera after the Cretaceous/Palaeogene boundary mass extinction. Hist. Biol. 29, 25-

928   42. https://doi.org/10.1080/08912963.2015.1119133.

929 Arenillas, I., Arz, J.A., Molina, E., 1998. El límite Cretácico/Terciario de Zumaya, Osinaga y

930   Músquiz (Pirineos): control bioestratigráfico y cuantitativo de hiatos con foraminíferos

931   planctónicos. Rev. Soc. Geol. Esp. 11(1-2), 127-138.

932 Arenillas, I., Arz, J.A., Molina, E., Dupuis, C., 2000a. The Cretaceous/Paleogene (K/P)

933   boundary at Aïn Settara, Tunisia: Sudden catastrophic mass extinction in planktic

934   foraminifera. J. Foraminifer. Res. 30, 202-218. https://doi.org/10.2113/0300202.

935 Arenillas, I., Arz, J.A., Molina, E., Dupuis, C., 2000b. An independent test of planktic

936   foraminiferal turnover across the Cretaceous/Paleogene (K/P) boundary at El Kef, Tunisia:

937   Catastrophic mass extinction and possible survivorship. Micropaleontology 46, 31-49.

938 Arenillas, I., Arz, J.A., Molina, E., 2004. A new high-resolution planktic foraminiferal zonation

939   and subzonation for the lower Danian. Lethaia 37, 79-95.

940   https://doi.org/10.1080/00241160310005097.

941 Arenillas, I., Arz, J.A., Grajales-Nishimura, J.M., Murillo-Muñetón, G., Alvarez, W., Camargo-

942   Zanoguera, A., Molina, E., Rosales-Domínguez, C., 2006. Chicxulub impact event is

943   Cretaceous/Paleogene boundary in age: New micropaleontological evidence. Earth Planet.

944   Sci. Lett. 249, 241-257. https://doi.org/10.1016/j.epsl.2006.07.020.

945 Arenillas, I., Arz, J.A., Grajales-Nishimura, J.M., Meléndez, A., Rojas-Consuegra, R., 2016.

946   The Chicxulub impact is synchronous with the planktonic foraminifera mass extinction at

947   the Cretaceous/Paleogene boundary: New evidence from the Moncada section, Cuba.

948   Geol. Acta 14, 35-51. https://doi.org/10.1344/GeologicaActa2016.14.1.4.

949 Arenillas, I., Arz, J.A., Gilabert, V., 2018. Blooms of aberrant planktic foraminifera across the

950   K/Pg boundary in the Western Tethys: Causes and evolutionary implications.

951   Paleobiology 44, 460-489. https://doi.org/10.1017/pab.2018.16.

952 Arz, J.A., Arenillas, I., Molina, E., Sepúlveda, R., 2000. La estabilidad evolutiva de los

953 foraminíferos planctónicos en el Maastrichtiense superior y su extinción en el límite

954 Cretácico/Terciario de Caravaca, España. Rev. geol. Chile 27, 27-47.

955 http://dx.doi.org/10.4067/S0716-02082000000100003.

956 Arz, J.A., Alegret, L., Arenillas, I., Liesa, C., Molina, E., Soria, A.R., 2001. Extinción de

957 foraminíferos del límite Cretácico/Terciario en Coxquihui (México) y su relación con las

958 evidencias de impacto. Rev. Esp. Micropaleontol. 33(2), 221-236.

959 Ashckenazi-Polivoda, S., Rak, C., Almogi-Labin, A., Zsolt, B., Ovadia, O., Abramovich, S.,

960 2014. Paleoecology of the K-Pg mass extinction survivor *Guembelitria* (Cushman):

961 isotopic evidence from pristine foraminifera from Brazos River, Texas (Maastrichtian).

962 Paleobiology 40, 24-33. https://doi.org/10.1666/13317.

963 Aze, T., Ezard, T.H.G., Purvis, A., Coxall, H.K., Stewart, D.R.M., Wade, B.S., Pearson, P.N.,

964 2011. A phylogeny of Cenozoic macroperforate planktonic foraminifera from fossil data.

965 Biol. Rev. 86, 900-927. https://doi.org/10.1111/j.1469-185X.2011.00178.x.

966 Ballent, S.C., Carignano, A.P., 2008. Morphological abnormalities in Late Cretaceous and early

967 Paleocene foraminifer tests (northern Patagonia, Argentina). Mar. Micropaleontol. 67,

968 288-296. https://doi.org/10.1016/j.marmicro.2008.02.003.

969 Baksi, A.K., 2001. The Rajahmundry Traps, Andhra Pradesh: Evaluation of their petrogenesis

970 relative to the Deccan Traps. Proc. Indian Acad. Sci. Earth Planet. Sci. 110, 397-407.

971 https://doi.org/10.1007/BF02702903.

972 Barnet, J.S.K., Littler, K., Kroon, D., Leng, M.J., Westerhold, T., Röhl, U., Zachos, J.C., 2018.

973 A new high-resolution chronology for the late Maastrichtian warming event: Establishing

974 robust temporal links with the onset of Deccan volcanism. Geology 46, 147-150.

975 https://doi.org/10.1130/G39771.1.

976   Barnet, J.S.K., Littler, K., Westerhold, T., Kroon, D., Leng, M.J., Bailey, I., Röhl, U., Zachos,

977   J.C., 2019. A High-Fidelity Benthic Stable Isotope Record of Late Cretaceous-Early

978   Eocene Climate Change and Carbon-Cycling. Paleoceanogr. Paleoclimatology 34, 672-

979   691. https://doi.org/10.1029/2019PA003556.

980   Beals, E.W., 1984. Bray-Curtis ordination: An effective strategy for analysis of multivariate

981   ecological data. Adv. Ecol. Res. 14, 1-55. https://doi.org/10.1016/S0065-2504(08)60168-

982   3.

983   Berger, W.H., Bonneau, M., Parker, F.L., Plateau, L., 1982. Foraminifera on the deep-sea floor:

984   lysocline and dissolution rate. Oceanol. Acta 5, 249-258.

985   Berggren, W.A., Pearson, P.N., 2005. A revised tropical to subtropical Paleogene planktonic

986   foraminiferal zonation. J. Foraminifer. Res. 35, 279-298. https://doi.org/10.2113/35.4.279.

987   Birch, H.S., Coxall, H.K., Pearson, P.N., 2012. Evolutionary ecology of Early Paleocene

988   planktonic foraminifera: size, depth habitat and symbiosis. Paleobiology 38, 374-390.

989   https://doi.org/10.1666/11027.1.

990   Birch, H.S., Coxall, H.K., Pearson, P.N., Kroon, D., Schmidt, D.N., 2016. Partial collapse of the

991   marine carbon pump after the Cretaceous-Paleogene boundary. Geology 44, 287-290.

992   https://doi.org/10.1130/G37581.1.

993   Boersma, A., Premoli Silva, I., 1989. Atlantic Paleogene biserial heterohelicid foraminifera and

994   oxygen minima. Paleoceanography 4, 271-286.

995   Bown, P., 2005. Selective calcareous nannoplankton survivorship at the Cretaceous-Tertiary

996   boundary. Geology 33, 653-656. https://doi.org/10.1130/G21566.1.

997   Burgess, S., 2019. Deciphering mass extinction triggers. Science 363, 815-816.

998   https://doi.org/10.1126/science.aaw0473.

999 Bralower, T.J., Cosmidis, J., Heaney, P.J., Kump, L.R., Morgan, J. V., Harper, D.T., Lyons,

1000   S.L., Freeman, K.H., Grice, K., Wendler, J.E., Zachos, J.C., Artemieva, N., Chen, S.A.,

1001   Gulick, S.P.S., House, C.H., Jones, H.L., Lowery, C.M., Nims, C., Schaefer, B., Thomas,

1002   E., Vajda, V., 2020. Origin of a global carbonate layer deposited in the aftermath of the

1003   Cretaceous-Paleogene boundary impact. Earth Planet. Sci. Lett. 548, 116476.

1004   https://doi.org/10.1016/j.epsl.2020.116476.

1005 Bukry, D., 1974. Coccoliths as paleosalinity indicators - evidence from Black Sea, in: Degens,

1006   E.T., Ross. D.A. (Eds.), The Black Sea–Geology, Chemistry, and Biology. AAPG Memoir

1007   20, Tulsa, pp. 353-363.

1008 Caldeira, K., Rampino, M.R., Volk, T., Zachos, J.C., 1990. Biogeochemical modeling at mass

1009   extinction boundaries: Atmospheric carbon dioxide and ocean alkalinity at the K/T

1010   boundary, in: Kauffman E.G., Walliser O.H. (Eds), Extinction Events in Earth History.

1011   Lecture Notes in Earth Sciences, 30, Springer, Berlin, Heidelberg, pp. 333-345.

1012   https://doi.org/10.1007/bfb0011156.

1013 Canudo, J.I., Keller, G., Molina, E., 1991. Cretaceous/Tertiary boundary extinction pattern and

1014   faunal turnover at Agost and Caravaca, S.E. Spain. Mar. Micropaleontol. 17, 319-341.

1015   https://doi.org/10.1016/0377-8398(91)90019-3.

1016 Chenet, A.L., Quidelleur, X., Fluteau, F., Courtillot, V., Bajpai, S., 2007. ^{40}K-^{40}Ar dating of the

1017   Main Deccan large igneous province: Further evidence of KTB age and short duration.

1018   Earth Planet. Sci. Lett. 263, 1-15. https://doi.org/10.1016/j.epsl.2007.07.011.

1019 Chiarenza, A.A., Farnsworth, A., Mannion, P.D., Lunt, D.J., Valdes, P.J., Morgan, J. V.,

1020   Allison, P.A., 2020. Asteroid impact, not volcanism, caused the end-Cretaceous dinosaur

1021   extinction. Proc. Natl. Acad. Sci. USA 117, 17084-17093.

1022   https://doi.org/10.1073/pnas.2006087117.

1023 Clyde, W.C., Ramezani, J., Johnson, K.R., Bowring, S.A., Jones, M.M., 2016. Direct high-

1024   precision U-Pb geochronology of the end-Cretaceous extinction and calibration of

1025   Paleocene astronomical timescales. Earth Planet. Sci. Lett. 452, 272-280.

1026   https://doi.org/10.1016/j.epsl.2016.07.041.

1027 Coccioni, R., Galeotti, S., 1994. K-T boundary extinction: Geologically instantaneous or

1028   gradual event? Evidence from deep-sea benthic foraminifera. Geology 22, 779-782.

1029   https://doi.org/10.1130/0091-7613(1994)022<0779:KTBEGI>2.3.CO;2.

1030 Coccioni, R., Luciani, V., 2006. *Guembelitria irregularis* bloom at the K-T boundary:

1031   Morphological abnormalities induced by impact-related extreme environmental stress?, in:

1032   Cockell, C., Gilmour, I., Koeberl, C. (Eds.), Biological Processes Associated with Impact

1033   Events. Springer-Verlag, Berlin, pp. 179-196. https://doi.org/10.1007/3-540-25736-5_8

1034 Coccioni, R., Frontalini, F., Bancalà, G., Fornaciari, E., Jovane, L., Sprovieri, M., 2010. The

1035   Dan-C2 hyperthermal event at Gubbio (Italy): Global implications, environmental effects,

1036   and cause(s). Earth Planet. Sci. Lett. 297, 298-305.

1037   https://doi.org/10.1016/j.epsl.2010.06.031.

1038 Courtillot, V., Besse, J., Vandamme, D., Montigny, R., Jaeger, J.-J., Cappetta, H., 1986. Deccan

1039   flood basalts at the Cretaceous/Tertiary boundary? Earth Planet. Sci. Lett. 80, 361–374.

1040 Courtillot, V., Fluteau, F., 2014. A review of the embedded time scales of flood basalt

1041   volcanism with special emphasis on dramatically short magmatic pulses, in: Keller, G.,

1042   Kerr, A.C. (Eds.), Volcanism, Impacts, and Mass Extinctions: Causes and Effects. Geol.

1043   Soc. Am. Spec. Pap. 505, p. 301-317. https://doi.org/10.1130/2014.2505(15).

1044 Coxall, H.K., D'Hondt, S., Zachos, J.C., 2006. Pelagic evolution and environmental recovery

1045   after the Cretaceous-Paleogene mass extinction. Geology 34, 297-300.

1046   https://doi.org/10.1130/G21702.1.

1047   Cunha, A.S., Shimabukuro, S., 1997. *Braarudosphaera* blooms and anomalous enrichments of

1048   *Nannoconus*: evidence from the Turonian South Atlantic, Santos Basin, Brazil. J.

1049   Nannoplankt. Res. 19, 51-55.

1050   D'Hondt, S., Donaghay, P., Zachos, J.C., Luttenberg, D., Lindinger, M., 1998. Organic carbon

1051   fluxes and ecological recovery from the Cretaceous-Tertiary mass extinction. Science 282,

1052   276-279. https://doi.org/10.1126/science.282.5387.276.

1053   Ellwood, B.B., Tomkin, J.H., Ratcliffe, K.T., Wright, M., Kafafy, A.M., 2008. High-resolution

1054   magnetic susceptibility and geochemistry for the Cenomanian/Turonian boundary GSSP

1055   with correlation to time equivalent core. Palaeogeogr. Palaeoclimatol. Palaeoecol. 261,

1056   105-126. https://doi.org/10.1016/j.palaeo.2008.01.005.

1057   Fendley, I.M., Sprain, C.J., Renne, P.R., Arenillas, I., Arz, J.A., Gilabert, V., Self, S.,

1058   Vanderkluysen, L., Pande, K., Smit, J., Mittal, T., 2020. No Cretaceous-Paleogene

1059   boundary in exposed Rajahmundry Traps: A refined chronology of the longest Deccan

1060   lava flows from ^{40}Ar/^{39}Ar dates, magnetostratigraphy, and biostratigraphy. Geochemistry,

1061   Geophys. Geosystems 21, 1-20. https://doi.org/10.1029/2020gc009149.

1062   Font, E., Adatte, T., Sial, A.N., de Lacerda, L.D., Keller, G., Punekar, J., 2016. Mercury

1063   anomaly, Deccan volcanism, and the end-Cretaceous mass extinction. Geology 44, 171-

1064   174. https://doi.org/10.1130/G37451.1.

1065   Font, E., Adatte, T., Andrade, M., Keller, G., Mbabi Bitchong, A., Carvallo, C., Ferreira, J.,

1066   Diogo, Z., Mirão, J., 2018. Deccan volcanism induced high-stress environment during the

1067   Cretaceous–Paleogene transition at Zumaia, Spain: Evidence from magnetic,

1068   mineralogical and biostratigraphic records. Earth Planet. Sci. Lett. 484, 53-66.

1069   https://doi.org/10.1016/j.epsl.2017.11.055.

1070

1071   Fornaciari, E., Giusberti, L., Luciani, V., Tateo, F., Agnini, C., Backman, J., Oddone, M., Rio,

1072   D., 2007. An expanded Cretaceous-Tertiary transition in a pelagic setting of the Southern

1073   Alps (central-western Tethys). Palaeogeogr. Palaeoclimatol. Palaeoecol. 255, 98-131.

1074   https://doi.org/10.1016/j.palaeo.2007.02.044.

1075   Gallala, N., Zaghbib-Turki, D., Arenillas, I., Arz, J.A., Molina, E., 2009. Catastrophic mass

1076   extinction and assemblage evolution in planktic foraminifera across the

1077   Cretaceous/Paleogene (K/Pg) boundary at Bidart (SW France). Mar. Micropaleontol. 72,

1078   196-209. https://doi.org/10.1016/j.marmicro.2009.05.001.

1079   Gardin, S., 2002. Late Maastrichtian to early Danian calcareous nannofossils at Elles

1080   (Northwest Tunisia). A tale of one million years across the K-T boundary. Palaeogeogr.

1081   Palaeoclimatol. Palaeoecol. 178, 211-231. https://doi.org/10.1016/S0031-0182(01)00397-

1082   2.

1083   Gardin, S., Monechi, S., 1998. Palaeoecological change in middle to low latitude calcareous

1084   nannoplankton at the Cretaceous/Tertiary boundary. Bull. Soc. géol. Fr. 169, 709-723.

1085   Gerstel, J., Thunell, R.C., Zachos, J.C., Arthur, M.A., 1986. The Cretaceous/Tertiary boundary

1086   event in the North Pacific: Planktonic foraminiferal results from Deep Sea Drilling Project

1087   Site 577, Shatsky Rise. Paleoceanography 1, 97-117.

1088   https://doi.org/10.1029/PA001i002p00097.

1089   Gertsch, B., Keller, G., Adatte, T., Garg, R., Prasad, V., Berner, Z., Fleitmann, D., 2011.

1090   Environmental effects of Deccan volcanism across the Cretaceous-Tertiary transition in

1091   Meghalaya, India. Earth Planet. Sci. Lett. 310, 272-285.

1092   https://doi.org/10.1016/j.epsl.2011.08.015.

1093   Gibbs, S.J., Bown, P.R., Ward, B.A., Alvarez, S.A., Kim, H., Archontikis, O.A., Sauterey, B.,

1094   Poulton, A.J., Wilson, J., Ridgwell, A., 2020. Algal plankton turn to hunting to survive

1095   and recover from end-Cretaceous impact darkness. Sci. Adv. 6, eabc9123.

1096   https://doi.org/10.1126/sciadv.abc9123.

1097   Gilabert, V., Arz, J.A., Arenillas, I., Robinson, S.A., 2021. Influence of the Latest Maastrichtian

1098   Warming Event on planktic foraminiferal assemblages and ocean carbonate saturation at

1099   Caravaca, Spain. Cretac. Res. 125, 104844. https://doi.org/10.1016/j.cretres.2021.104844

1100   Groot, J.J., de Jonge, R.B.G., Langereis, C.G., ten Kate, W.G.H.Z., Smit, J., 1989.

1101   Magnetostratigraphy of the Cretaceous-Tertiary boundary at Agost (Spain). Earth Planet.

1102   Sci. Lett. 94, 385-397. https://doi.org/10.1016/0012-821X(89)90155-6.

1103   Gulick, S.P.S., Bralower, T.J., Ormö, J., Hall, B., Grice, K., Schaefer, B., Lyons, S., Freeman,

1104   K.H., Morgan, J. V., Artemieva, N., Kaskes, P., De Graaff, S.J., Whalen, M.T., Collins,

1105   G.S., Tikoo, S.M., Verhagen, C., Christeson, G.L., Claeys, P., Coolen, M.J.L., Goderis, S.,

1106   Goto, K., Grieve, R.A.F., McCall, N., Osinski, G.R., Rae, A.S.P., Riller, U., Smit, J.,

1107   Vajda, V., Wittmann, A., 2019. The first day of the Cenozoic. Proc. Natl. Acad. Sci. USA

1108   116, 19342-19351. https://doi.org/10.1073/pnas.1909479116.

1109   Hammer, Ø., Harper, D.A.T., Ryan, P.D., 2001. PAST: Paleontological statistics software

1110   package for education and data analysis. Paleontol. Electron. 4 (1), 9.

1111   Henehan, M.J., Hull, P.M., Penman, D.E., Rae, J.W.B., Schmidt, D.N., 2016. Biogeochemical

1112   significance of pelagic ecosystem function: An end-Cretaceous case study. Philos. Trans.

1113   R. Soc. B Biol. Sci. 371. https://doi.org/10.1098/rstb.2015.0510.

1114   Henehan, M.J., Ridgwell, A., Thomas, E., Zhang, S., Alegret, L., Schmidt, D.N., Rae, J.W.B.,

1115   Witts, J.D., Landman, N.H., Greene, S.E., Huber, B.T., Super, J.R., Planavsky, N.J., Hull,

1116   P.M., 2019. Rapid ocean acidification and protracted Earth system recovery followed the

1117   end-Cretaceous Chicxulub impact. Proc. Natl. Acad. Sci. USA 116, 22500-22504.

1118   https://doi.org/10.1073/pnas.1905989116.

1119   Hernandez Nava, A., Black, B.A., Gibson, S.A., Bodnar, R.J., Renne, P.R., Vanderkluysen, L.,

1120   2021. Reconciling early Deccan Traps CO_2 outgassing and pre-KPB global climate. Proc.

1121   Natl. Acad. Sci. USA 118, e2007797118. https://doi.org/10.1073/pnas.2007797118.

1122   Hildebrand, A.R., Penfield, G.T., Kring, D.A., Pilkington, M., Antonio, C.Z., Boynton, W. V.,

1123   1991. Chicxulub crater: A possible Cretaceous/Tertiary boundary impact crater on the

1124   Yucatan peninsula, Mexico. Geology 19, 867-871. https://doi.org/10.1130/0091-

1125   7613(1991)019<0867:CCAPCT>2.3.CO;2.

1126   Huber, B.T., MacLeod, K.G., Norris, R.D., 2002. Abrupt extinction and subsequent reworking

1127   of Cretaceous planktonic foraminifera across the Cretaceous-Tertiary boundary: Evidence

1128   from the subtropical North Atlantic. Geol. Soc. Am. Spec. Pap. 356, 277-289.

1129   https://doi.org/10.1130/0-8137-2356-6.277.

1130   Hull, P.M., Bornemann, A., Penman, D.E., Henehan, M.J., Norris, R.D., Wilson, P.A., Blum,

1131   P., Alegret, L., Batenburg, S.J., Bown, P.R., Bralower, T.J., Cournede, C., Deutsch, A.,

1132   Donner, B., Friedrich, O., Jehle, S., Kim, H., Kroon, D., Lippert, P.C., Loroch, D.,

1133   Moebius, I., Moriya, K., Peppe, D.J., Ravizza, G.E., Röhl, U., Schueth, J.D., Sepúlveda, J.,

1134   Sexton, P.F., Sibert, E.C., Śliwińska, K.K., Summons, R.E., Thomas, E., Westerhold, T.,

1135   Whiteside, J.H., Yamaguchi, T., Zachos, J.C., 2020. On impact and volcanism across the

1136   Cretaceous-Paleogene boundary. Science 367, 266-272.

1137   https://doi.org/10.1126/science.aay5055.

1138   Jay, A.E., Widdowson, M., 2008. Stratigraphy, structure and volcanology of the SE Deccan

1139   continental flood basalt province: Implications for eruptive extent and volumes. J. Geol.

1140   Soc. London. 165, 177-188. https://doi.org/10.1144/0016-76492006-062.

1141   Jiang, S., Bralower, T.J., Patzkowsky, M.E., Kump, L.R., Schueth, J.D., 2010. Geographic

1142   controls on nannoplankton extinction across the Cretaceous/Palaeogene boundary. Nat.

1143   Geosci. 3, 280-285. https://doi.org/10.1038/ngeo775.

1144 Jiang, S., Chen, X., Bernaola, G., 2019. Environmental controls on calcareous nannoplankton

1145   response to the Cretaceous/Paleogene mass extinction in the Tethys realm. Palaeogeogr.

1146   Palaeoclimatol. Palaeoecol. 515, 134-142. https://doi.org/10.1016/j.palaeo.2017.12.044.

1147 Jones, H.L., Lowery, C.M., Bralower, T.J., 2019. Delayed calcareous nannoplankton boom-bust

1148   successions in the earliest Paleocene Chicxulub (Mexico) impact crater. Geology 47, 753-

1149   756. https://doi.org/10.1130/G46143.1.

1150 Kaiho, K., Lamolda, M.A., 1999. Catastrophic extinction of planktonic foraminifera at the

1151   Cretaceous-Tertiary boundary evidenced by stable isotopes and foraminiferal abundance at

1152   Caravaca, Spain. Geology 27, 355-358. https://doi.org/10.1130/0091-

1153   7613(1999)027<0355:CEOPFA>2.3.CO;2.

1154 Kaiho, K., Kajiwara, Y., Tazaki, K., Ueshima, M., Takeda, N., Kawahata, H., Arinobu, T.,

1155   Ishiwatari, R., Hirai, A., Lamolda, M.A., 1999. Oceanic primary productivity and

1156   dissolved oxygen levels at the Cretaceous/Tertiary boundary: Their decrease, subsequent

1157   warming, and recovery. Paleoceanography 14, 511-524.

1158   https://doi.org/10.1029/1999PA900022.

1159 Kasbohm, J., Schoene, B., Burgess, S., 2021. Radiometric constraints on the timing, tempo, and

1160   effects of large igneous province emplacement, in: Ernst, R.E., Dickson, J., Bekker, A.

1161   (Eds.), Large Igneous Provinces: A Driver of Global Environmental and Biotic Changes.

1162   American Geophysical Union. Carbon in Earth's Interior published by John Wiley & Sons,

1163   Inc., pp. 27-82. https://doi.org/https://doi.org/10.1002/9781119507444.ch2.

1164 Kawaragi, K., Sekine, Y., Kadono, T., Sugita, S., Ohno, S., Ishibashi, K., Kurosawa, K., Matsui,

1165   T., Ikeda, S., 2009. Direct measurements of chemical composition of shock-induced gases

1166   from calcite: an intense global warming after the Chicxulub impact due to the indirect

1167   greenhouse effect of carbon monoxide. Earth Planet. Sci. Lett. 282, 56-64.

1168   https://doi.org/10.1016/j.epsl.2009.02.037.

1169   Keller, G., 2003. *Guembelitria* dominated late Maastrichtian planktic foraminiferal

1170   assemblages mimic early Danian in central Egypt. Mar. Micropaleontol. 47, 71-99.

1171   https://doi.org/10.1016/S0377-8398(02)00116-0.

1172   Keller, G., Pardo, A., 2004. Disaster opportunists Guembelitrinidae: Index for environmental

1173   catastrophes. Mar. Micropaleontol. 53, 83-116.

1174   https://doi.org/10.1016/j.marmicro.2004.04.012.

1175   Keller, G., Adatte, T., Gardin, S., Bartolini, A., Bajpai, S., 2008. Main Deccan volcanism phase

1176   ends near the K-T boundary: Evidence from the Krishna-Godavari Basin, SE India. Earth

1177   Planet. Sci. Lett. 268, 293-311. https://doi.org/10.1016/j.epsl.2008.01.015.

1178   Keller, G.K., Bhowmick, P.K., Upadhyay, H., Dave, A., Reddy, A.N., Jaiprakash, B.C., Adatte,

1179   T., 2011. Deccan volcanism linked to the Cretaceous-Tertiary boundary mass extinction:

1180   New evidence from ONGC wells in the Krishna-Godavari Basin. J. Geol. Soc. India 78,

1181   399-428. https://doi.org/10.1007/s12594-011-0107-3.

1182   Keller, G., Adatte, T., Bhowmick, P.K., Upadhyay, H., Dave, A., Reddy, A.N., Jaiprakash,

1183   B.C., 2012. Nature and timing of extinctions in Cretaceous-Tertiary planktic foraminifera

1184   preserved in Deccan intertrappean sediments of the Krishna-Godavari Basin, India. Earth

1185   Planet. Sci. Lett. 341-344, 211-221. https://doi.org/10.1016/j.epsl.2012.06.021.

1186   Keller, G., Punekar, J., Mateo, P., 2016. Upheavals during the Late Maastrichtian: Volcanism,

1187   climate and faunal events preceding the end-Cretaceous mass extinction. Palaeogeogr.

1188   Palaeoclimatol. Palaeoecol. 441, 137-151. https://doi.org/10.1016/j.palaeo.2015.06.034.

1189   Keller, G., Mateo, P., Monkenbusch, J., Thibault, N., Punekar, J., Spangenberg, J.E.,

1190   Abramovich, S., Ashckenazi-Polivoda, S., Schoene, B., Eddy, M.P., Samperton, K.M.,

1191   Khadri, S.F.R., Adatte, T., 2020. Mercury linked to Deccan Traps volcanism, climate

1192   change and the end-Cretaceous mass extinction. Glob. Planet. Change 194, 103312.

1193   https://doi.org/10.1016/j.gloplacha.2020.103312.

1194   Kelly, D.C., Norris, R.D., Zachos, J.C., 2003. Deciphering the paleoceanographic significance

1195   of Early Oligocene *Braarudosphaera* chalks in the South Atlantic. Mar. Micropaleontol.

1196   49, 49-63. https://doi.org/10.1016/S0377-8398(03)00027-6.

1197   Krahl, G., Bom, M.H.H., Kochhann, K.G.D., Souza, L. V., Savian, J.F., Fauth, G., 2020.

1198   Environmental changes occurred during the early Danian at the Rio Grande Rise, South

1199   Atlantic Ocean. Glob. Planet. Change 191, 103197.

1200   https://doi.org/10.1016/j.gloplacha.2020.103197.

1201   Kring, D.A., 2007. The Chicxulub impact event and its environmental consequences at the

1202   Cretaceous-Tertiary boundary. Palaeogeogr. Palaeoclimatol. Palaeoecol. 255, 4-21.

1203   https://doi.org/10.1016/j.palaeo.2007.02.037.

1204   Kroon, D., Nederbragt, A.J., 1990. Ecology and paleoecology of triserial planktic foraminifera.

1205   Mar. Micropaleontol. 16, 25-38. https://doi.org/10.1016/0377-8398(90)90027-J.

1206   Kucera, M., Malmgren, B.A., Sturesson, U., 1997. Foraminiferal dissolution at shallow depths

1207   of the Walvis Ridge and Rio Grande Rise during the latest Cretaceous: Inferences for

1208   deep-water circulation in the South Atlantic. Palaeogeogr. Palaeoclimatol. Palaeoecol.

1209   129, 195-212. https://doi.org/10.1016/S0031-0182(96)00133-2.

1210   Lamolda, M.A., Melinte, M.C., Kaiho, K., 2005. Nannofloral extinction and survivorship across

1211   the K/T boundary at Caravaca, southeastern Spain. Palaeogeogr. Palaeoclimatol.

1212   Palaeoecol. 224, 27-52. https://doi.org/10.1016/j.palaeo.2005.03.030.

1213   Lamolda, M.A., Melinte-Dobrinescu, M.C., Kaiho, K., 2016. Calcareous nannoplankton

1214   assemblage changes linked to paleoenvironmental deterioration and recovery across the

1215   Cretaceous-Paleogene boundary in the Betic Cordillera (Agost, Spain). Palaeogeogr.

1216   Palaeoclimatol. Palaeoecol. 441, 438-452. https://doi.org/10.1016/j.palaeo.2015.10.003.

1217   Legendre, P., Gallagher, E.D., 2001. Ecologically meaningful transformations for ordination of

1218   species data. Oecologia 129, 271-280. https://doi.org/10.1007/s004420100716.

1219   Lowery, C.M., Fraass, A.J., 2019. Morphospace expansion paces taxonomic diversification

1220   after end Cretaceous mass extinction. Nat. Ecol. Evol. 3, 900-904.

1221   https://doi.org/10.1038/s41559-019-0835-0.

1222   Lowery, C.M., Bralower, T.J., Owens, J.D., Rodríguez-Tovar, F.J., Jones, H., Smit, J., Whalen,

1223   M.T., Claeys, P., Farley, K., Gulick, S.P.S., Morgan, J. V., Green, S., Chenot, E.,

1224   Christeson, G.L., Cockell, C.S., Coolen, M.J.L., Ferrière, L., Gebhardt, C., Goto, K.,

1225   Kring, D.A., Lofi, J., Ocampo-Torres, R., Perez-Cruz, L., Pickersgill, A.E., Poelchau,

1226   M.H., Rae, A.S.P., Rasmussen, C., Rebolledo-Vieyra, M., Riller, U., Sato, H., Tikoo,

1227   S.M., Tomioka, N., Urrutia-Fucugauchi, J., Vellekoop, J., Wittmann, A., Xiao, L.,

1228   Yamaguchi, K.E., Zylberman, W., 2018. Rapid recovery of life at ground zero of the end-

1229   Cretaceous mass extinction. Nature 558, 288-291. https://doi.org/10.1038/s41586-018-

1230   0163-6.

1231   Lowery, C.M., Bown, P.R., Fraass, A.J., Hull, P.M., 2020. Ecological Response of Plankton to

1232   Environmental Change: Thresholds for Extinction. Annu. Rev. Earth Planet. Sci. 48.

1233   https://doi.org/10.1146/annurev-earth-081619-052818.

1234   Luciani, V., D'Onofrio, R., Filippi, G., Moretti, S., 2020. Which was the habitat of early Eocene

1235   planktic foraminifer *Chiloguembelina*? Stable isotope paleobiology from the Atlantic

1236   Ocean and implication for paleoceanographic reconstructions. Glob. Planet. Change 191,

1237   103216. https://doi.org/10.1016/j.gloplacha.2020.103216.

1238   Lyson, T.R., Miller, I.M., Bercovici, A.D., Weissenburger, K., Fuentes, A.J., Clyde, W.C.,

1239   Hagadorn, J.W., Butrim, M.J., Johnson, K.R., Fleming, R.F., Barclay, R.S., Maccracken,

1240   S.A., Lloyd, B., Wilson, G.P., Krause, D.W., Chester, S.G.B., 2019. Exceptional

1241   continental record of biotic recovery after the Cretaceous−Paleogene mass extinction.

1242   Science 366, 977-983. https://doi.org/10.1126/science.aay2268.

1243   Mateo, P., Keller, G., Adatte, T., Spangenberg, J.E., 2016. Mass wasting and hiatuses during the

1244   Cretaceous-Tertiary transition in the North Atlantic: Relationship to the Chicxulub

1245   impact? Palaeogeogr. Palaeoclimatol. Palaeoecol. 441, 96-115.

1246   https://doi.org/10.1016/j.palaeo.2015.01.019.

1247   Metsana-Oussaid, F., Belhai, D., Arenillas, I., Arz, J.A., Gilabert, V., 2019. New sections of the

1248   Cretaceous-Paleogene transition in the southwestern Tethys (Médéa, northern Algeria):

1249   planktic foraminiferal biostratigraphy and biochronology. Arab. J. Geosci. 12.

1250   https://doi.org/10.1007/s12517-019-4402-4.

1251   Minoletti, F., De Rafelis, M., Renard, M., Gardin, S., Young, J., 2005. Changes in the pelagic

1252   fine fraction carbonate sedimentation during the Cretaceous-Paleocene transition:

1253   Contribution of the separation technique to the study of Bidart section. Palaeogeogr.

1254   Palaeoclimatol. Palaeoecol. 216, 119-137. https://doi.org/10.1016/j.palaeo.2004.10.006.

1255   Molina, E., Arenillas, I., Arz, J.A. 1998. Mass extinction in planktic foraminifera at the

1256   Cretaceous/Tertiary boundary in subtropical and temperate latitudes. Bull. Soc. géol. Fr.

1257   169(3), 351-363.

1258   Molina, E., Alegret, L., Arenillas, I., Arz, J.A., Gallala, N., Grajales-Nishimura, J.M., Murillo-

1259   Muñetón, G., Zaghbib-Turki, D., 2009. The Global Boundary Stratotype Section and Point

1260   for the base of the Danian Stage (Paleocene, Paleogene, "Tertiary", Cenozoic): Auxiliary

1261   sections and correlation. Episodes 32, 84-95.

1262   https://doi.org/10.18814/epiiugs/2009/v32i2/002.

1263   Mukhopadhyay, S., Farley, KA., Montanari, A., 2001. A short duration of the Cretaceous-

1264   Tertiary boundary event: Evidence from extraterrestrial Helium[3]. Science 291, 1952-1955.

1265   https://doi.org/10.1126/science.291.5510.1952

1266   Norris, R.D., 1996. Symbiosis as an evolutionary innovation in the radiation of Paleocene

1267   planktic foraminifera. Paleobiology 22, 461-480.

1268   https://doi.org/10.1017/S0094837300016468.

1269   Olsson, R.K., Berggren, W.A., Hemleben, C., Huber, B.T., 1999. Atlas of Paleocene Planktonic

1270   Foraminifera. Smithson. Contrib. to Paleobiol. 85, 1-252.

1271   https://doi.org/10.5479/si.00810266.85.1.

1272   Omaña, L., Alencáster, G., Hernández, J.R.T., Doncel, R.L., 2012. Morphological abnormalities

1273   and dwarfism in Maastrichtian foraminifera from the Cárdenas Formation, Valles-San

1274   Luis Potosí Platform, Mexico: Evidence of paleoenvironmental stress. Bol. Soc. Geol.

1275   Mex. 64, 305-318. https://doi.org/10.18268/BSGM2012v64n3a4.

1276   Pardo, A., Keller, G., 2008. Biotic effects of environmental catastrophes at the end of the

1277   Cretaceous and early Tertiary: *Guembelitria* and *Heterohelix* blooms. Cretac. Res. 29,

1278   1058-1073. https://doi.org/10.1016/j.cretres.2008.05.031.

1279   Pospichal, J.J., 1996. Calcareous nannoplankton mass extinction at the Cretaceous/Tertiary

1280   boundary: An update. Geol. Soc. Am. Spec. Pap. 307, 335-360. https://doi.org/10.1130/0-

1281   8137-2307-8.335.

1282   Premović, P.I., 2009. Experimental evidence for the global acidification of surface ocean at the

1283   Cretaceous-Palaeogene boundary: The biogenic calcite-poor spherule layers. Int. J.

1284   Astrobiol. 8, 193-206. https://doi.org/10.1017/S1473550409990139.

1285 Punekar, J., Mateo, P., Keller, G., 2014a. Effects of Deccan volcanism on paleoenvironment

1286 and planktic foraminifera: A global survey. Spec. Geol. Soc. Am. Spec. Pap. 505, 91-116.

1287 https://doi.org/10.1130/2014.2505(04).

1288 Punekar, J., Keller, G., Khozyem, H., Hamming, C., Adatte, T., Tantawy, A.A., Spangenberg,

1289 J.E., 2014b. Late Maastrichtian-early Danian high-stress environments and delayed

1290 recovery linked to Deccan volcanism. Cretac. Res. 49, 63-82.

1291 https://doi.org/10.1016/j.cretres.2014.01.002.

1292 Punekar, J., Keller, G., Khozyem, H.M., Adatte, T., Font, E., Spangenberg, J., 2016. A multi-

1293 proxy approach to decode the end-Cretaceous mass extinction. Palaeogeogr.

1294 Palaeoclimatol. Palaeoecol. 441, 116-136. https://doi.org/10.1016/j.palaeo.2015.08.025.

1295 Quillévéré, F., Norris, R.D., Kroon, D., Wilson, P.A., 2008. Transient ocean warming and shifts

1296 in carbon reservoirs during the early Danian. Earth Planet. Sci. Lett. 265, 600-615.

1297 https://doi.org/10.1016/j.epsl.2007.10.040.

1298 Renne, P.R., Sprain, C.J., Richards, M.A., Self, S., Vanderkluysen, L., Pande, K., 2015. State

1299 shift in Deccan volcanism at the Cretaceous-Paleogene boundary, possibly induced by

1300 impact. Science 350, 76-78. https://doi.org/10.1126/science.aac7549.

1301 Renne, P.R., Arenillas, I., Arz, J.A., Vajda, V., Gilabert, V., Bermúdez, H.D., 2018. Multi-

1302 proxy record of the Chicxulub impact at the Cretaceous- Paleogene boundary from

1303 Gorgonilla Island, Colombia. Geology 46, 547-550. https://doi.org/10.1130/G40224.1.

1304 Ricotta, C., Podani, J., 2017. On some properties of the Bray-Curtis dissimilarity and their

1305 ecological meaning. Ecol. Complex. 31, 201-205.

1306 https://doi.org/10.1016/j.ecocom.2017.07.003.

1307 Richards, M.A., Alvarez, W., Self, S., Karlstrom, L., Renne, P.R., Manga, M., Sprain, C.J.,

1308 Smit, J., Vanderkluysen, L., Gibson, S.A., 2015. Triggering of the largest Deccan

1309   eruptions by the Chicxulub impact. Bull. Geol. Soc. Am. 127, 1507-1520.

1310   https://doi.org/10.1130/B31167.1.

1311   Robinson, N., Ravizza, G., Coccioni, R., Peucker-Ehrenbrink, B., Norris, R., 2009. A high-

1312   resolution marine ^{187}Os/^{188}Os record for the late Maastrichtian: Distinguishing the

1313   chemical fingerprints of Deccan volcanism and the K-P impact event. Earth Planet. Sci.

1314   Lett. 281, 159-168. https://doi.org/10.1016/j.epsl.2009.02.019.

1315   Romein, A.J.T., 1977. Calcareous nannofossils from the Cretaceous/Tertiary boundary interval

1316   in the Barranco del Gredero (Caravaca, Prov. Murcia, SE Spain). Proc. K. Ned. Akad.

1317   Wet. Ser. B 80, 256-279.

1318   Schmidt, A., Skeffington, R.A., Thordarson, T., Self, S., Forster, P.M., Rap, A., Ridgwell, A.,

1319   Fowler, D., Wilson, M., Mann, G.W., Wignall, P.B., Carslaw, K.S., 2016. Selective

1320   environmental stress from sulphur emitted by continental flood basalt eruptions. Nat.

1321   Geosci. 9, 77-82. https://doi.org/10.1038/ngeo2588.

1322   Schoene, B., Samperton, K.M., Eddy, M.P., Keller, G., Adatte, T., Bowring, S.A., Khadri,

1323   S.F.R., Gertsch, B., 2015. U-Pb geochronology of the Deccan Traps and relation to the

1324   end-Cretaceous mass extinction. Science 347, 182-184.

1325   https://doi.org/10.1126/science.aaa0118.

1326   Schoene, B., Eddy, M.P., Samperton, K.M., Keller, C.B., Keller, G., Adatte, T., Khadri, S.F.R.,

1327   2019. U-Pb constraints on pulsed eruption of the Deccan Traps across the end-Cretaceous

1328   mass extinction. Science 363, 862-866. https://doi.org/10.1126/science.aau2422.

1329   Schoene, B., Eddy, M. P., Keller, C. B., and Samperton, K. M., 2021. An evaluation of Deccan

1330   Traps eruption rates using geochronologic data: Geochronology 3, 181–198.

1331   https://doi.org/10.5194/gchron-3-181-2021.

1332 Schulte, P., Alegret, L., Arenillas, I., Arz, J.A., Barton, P.J., Bown, P.R., Bralower, T.J.,

1333   Christeson, G.L., Claeys, P., Cockell, C.S., Collins, G.S., Deutsch, A., Goldin, T.J., Goto,

1334   K., Grajales-Nishimura, J.M., Grieve, R.A.F., Gulick, S.P.S., Johnson, K.R., Kiessling,

1335   W., Koeberl, C., Kring, D.A., MacLeod, K.G., Matsui, T., Melosh, J., Montanari, A.,

1336   Morgan, J. V., Neal, C.R., Nichols, D.J., Norris, R.D., Pierazzo, E., Ravizza, G.,

1337   Rebolledo-Vieyra, M., Reimold, W.U., Robin, E., Salge, T., Speijer, R.P., Sweet, A.R.,

1338   Urrutia-Fucugauchi, J., Vajda, V., Whalen, M.T., Willumsen, P.S., 2010. The Chicxulub

1339   asteroid impact and mass extinction at the Cretaceous-Paleogene boundary. Science 327,

1340   1214-1218. https://doi.org/10.1126/science.1177265.

1341 Self, S., Widdowson, M., Thordarson, T., Jay, A.E., 2006. Volatile fluxes during flood basalt

1342   eruptions and potential effects on the global environment: A Deccan perspective. Earth

1343   Planet. Sci. Lett. 248, 518-532. https://doi.org/10.1016/j.epsl.2006.05.041.

1344 Self, S., Jay, A.E., Widdowson, M., Keszthelyi, L.P., 2008. Correlation of the Deccan and

1345   Rajahmundry Trap lavas: Are these the longest and largest lava flows on Earth? J.

1346   Volcanol. Geotherm. Res. 172, 3-19. https://doi.org/10.1016/j.jvolgeores.2006.11.012.

1347 Sepúlveda, J., Wendler, J.E., Summons, R.E., Hinrichs, K.U., 2009. Rapid resurgence of marine

1348   productivity after the Cretaceous-Paleogene mass extinction. Science 326, 129-132.

1349   https://doi.org/10.1126/science.1176233.

1350 Sepúlveda, J., Alegret, L., Thomas, E., Haddad, E., Cao, C., Summons, R.E., 2019. Stable

1351   Isotope Constraints on Marine Productivity Across the Cretaceous-Paleogene Mass

1352   Extinction. Paleoceanogr. Paleoclimatology 34, 1195-1217.

1353   https://doi.org/10.1029/2018PA003442.

1354 Sinnesael, M., Montanari, A., Coccioni, R., Frontalini, F., Gattacceca, J., Snoeck, C., Wegner,

1355   W., Koeberl, C., Morgan, L.E., De Winter, N.J., DePaolo, D.J., Claeys, P., 2019.

1356   Multiproxy Cretaceous-Paleogene boundary event stratigraphy: An Umbria-Marche

1357   basinwide perspective. Geol. Soc. Am. Spec. Pap. 542, 133-158.

1358   https://doi.org/10.1130/2019.2542(07).

1359   Smit, J., 1982. Extinction and evolution of planktonic foraminifera after a major impact at the

1360   Cretaceous/Tertiary boundary. Geol. Soc. Am. Spec. Pap. 190, 329-352.

1361   https://doi.org/10.1130/SPE190-p329.

1362   Smit, J., 1999. The global stratigraphy of the Cretaceous-Tertiary boundary impact ejecta.

1363   Annu. Rev. Earth Planet. Sci. 27, 75-113. https://doi.org/10.1146/annurev.earth.27.1.75.

1364   Smit, J., 2004. The section of the Barranco del Gredero (Caravaca, SE Spain): A crucial section

1365   for the Cretaceous/Tertiary boundary impact extinction hypothesis. J. Iber. Geol. 31, 179-

1366   191. https://doi.org/10.5209/JIGE.33967.

1367   Smit, J., Hertogen, J., 1980. An extraterrestrial event at the Cretaceous-Tertiary boundary.

1368   Nature 285, 198-200. https://doi.org/10.1038/285198a0.

1369   Smit, J., Romein, A.J.T., 1985. A sequence of events across the Cretaceous-Tertiary boundary.

1370   Earth Planet. Sci. Lett. 74, 155-170. https://doi.org/10.1016/0012-821X(85)90019-6.

1371   Sosa-Montes de Oca, C., Rodríguez-Tovar, F.J., Martínez-Ruiz, F., 2016. Geochemical and

1372   isotopic characterization of trace fossil infillings: New insights on tracemaker activity after

1373   the K/Pg impact event. Cretac. Res. 57, 391-401.

1374   https://doi.org/10.1016/j.cretres.2015.03.003.

1375   Sprain, C.J., Renne, P.R., Clemens, W.A., Wilson, G.P., 2018. Calibration of chron C29r: New

1376   high-precision geochronologic and paleomagnetic constraints from the Hell Creek region,

1377   Montana. Bull. Geol. Soc. Am. 130, 1615-1644. https://doi.org/10.1130/B31890.1.

1378   Sprain, C.J., Renne, P.R., Vanderkluysen, L., Pande, K., Self, S., Mittal, T., 2019. The eruptive

1379   tempo of Deccan volcanism in relation to the Cretaceous-Paleogene boundary. Science.

1380   363, 866-870. https://doi.org/10.1126/science.aav1446.

1381   Stax, R., Stein, R., 1993. Long-term changes in the accumulation of organic carbon in Neogene

1382   sediments, Ontong Java Plateau. Proc., Sci. results, ODP, Leg 130, Ontong Java Plateau

1383   130, 573-584. https://doi.org/10.2973/odp.proc.sr.130.039.1993.

1384   Steinthorsdottir, M., Vajda, V., Pole, M., 2016. Global trends of pCO_2 across the Cretaceous-

1385   Paleogene boundary supported by the first Southern Hemisphere stomatal proxy-based

1386 pCO_2 reconstruction. Palaeogeogr. Palaeoclimatol. Palaeoecol. 464, 143-152.

1387   https://doi.org/10.1016/j.palaeo.2016.04.033.

1388   Thibault, N., Gardin, S., 2010. The calcareous nannofossil response to the end-Cretaceous warm

1389   event in the Tropical Pacific. Palaeogeogr. Palaeoclimatol. Palaeoecol. 291, 239-252.

1390   https://doi.org/10.1016/j.palaeo.2010.02.036.

1391   Thibault, N., Galbrun, B., Gardin, S., Minoletti, F., Le Callonnec, L., 2016. The end-Cretaceous

1392   in the southwestern Tethys (Elles, Tunisia): orbital calibration of paleoenvironmental

1393   events before the mass extinction. Int. J. Earth Sci. 105, 771-795.

1394   https://doi.org/10.1007/s00531-015-1192-0.

1395   Thibault, N., Minoletti, F., Gardin, S., 2018. Offsets in the early Danian recovery phase in

1396   carbon isotopes: Evidence from the biometrics and phylogeny of the *Cruciplacolithus*

1397   lineage. Rev. Micropaleontol. 61, 207-221. https://doi.org/10.1016/j.revmic.2018.09.002.

1398   Tobin, T.S., Bitz, C.M., Archer, D., 2017. Modeling climatic effects of carbon dioxide

1399   emissions from Deccan Traps volcanic eruptions around the Cretaceous-Paleogene

1400   boundary. Palaeogeogr. Palaeoclimatol. Palaeoecol. 478, 139-148.

1401   https://doi.org/10.1016/j.palaeo.2016.05.028.

1402   Vandamme, D., Courtillot, V., Besse, J., Montigny, R., 1991. Paleomagnetism and age

1403   determinations of the Deccan traps (India): results of a Nagpur–Bombay traverse and

1404   review of earlier work. Rev. Geophys. Space Phys. 29, 159–190.

1405   Vellekoop, J., Sluijs, A., Smit, J., Schouten, S., Weijers, J.W.H., Sinninghe Damsté, J.S.,

1406   Brinkhuis, H., 2014. Rapid short-term cooling following the Chicxulub impact at the

1407   Cretaceous-Paleogene boundary. Proc. Natl. Acad. Sci. USA 111, 7537-7541.

1408   https://doi.org/10.1073/pnas.1319253111.

1409   Vellekoop, J., Esmeray-Senlet, S., Miller, K.G., Browning, J. V, Sluijs, A., van de

1410   Schootbrugge, B., Sinninghe Damsté, J.S., Brinkhuis, H., 2016. Evidence for Cretaceous-

1411   Paleogene boundary bolide "impact winter" conditions from New Jersey, USA. Geology

1412   44. https://doi.org/10.1130/G37961.1.

1413   Vellekoop, J., Woelders, L., van Helmond, N.A.G.M., Galeotti, S., Smit, J., Slomp, C.P.,

1414   Brinkhuis, H., Claeys, P., Speijer, R.P., 2018. Shelf hypoxia in response to global warming

1415   after the Cretaceous-Paleogene boundary impact. Geology 46, 683-686.

1416   https://doi.org/10.1130/G45000.1.

1417   Wade, B.S., Pearson, P.N., Berggren, W.A., Pälike, H., 2011. Review and revision of Cenozoic

1418   tropical planktonic foraminiferal biostratigraphy and calibration to the geomagnetic

1419   polarity and astronomical time scale. Earth-Science Rev. 104, 111-142.

1420   https://doi.org/10.1016/j.earscirev.2010.09.003.